

IPAS-HEP-k007  
Jan 2001  
rev. Apr 2001

## $\mu \rightarrow e \gamma$ from Supersymmetry without R-parity

**Kingman Cheung<sup>1</sup> and Otto C. W. Kong<sup>2</sup>**

<sup>1</sup> *National Center for Theoretical Science, NTHU, Hsinchu, Taiwan*

<sup>2</sup> *Institute of Physics, Academia Sinica, Nankang, Taipei, Taiwan 11529*

### Abstract

Starting from the new sources of *LL*- and *LR*- scalar (slepton) mixings due to the R-parity violation, we discuss the structure of lepton-flavor violation focusing on the radiative decay of a muon into an electron. Using an optimal parametrization, we give the general formulas for the one-loop contributions, from which we discuss all combinations of R-parity violating parameters that possibly have a substantial contribution to the  $\mu \rightarrow e \gamma$  decay width. An exact numerical study is performed to obtain explicit bounds on the parameters under the present experimental limit. The most interesting one involves a combination of bilinear and trilinear couplings.

## I. INTRODUCTION

The standard model (SM) is built upon the fact that neutrinos have no right-handed components and are massless. Thus, lepton flavors are conserved. So far, experiments have not yet observed any lepton-flavor violation (LFV). Nevertheless, the evidence of small neutrino masses (implied from oscillation analyses of solar and atmospheric neutrino data [1]) implies a small amount of LFV. Many new physics models beyond the SM predict a certain amount of LFV, in relation to neutrino mass generation or otherwise. An important criterion for a viable model is that it should give an acceptable neutrino mass spectrum while staying within the experimental limits of LFV. Among the latter processes, the radiative decay of muon,  $\mu \rightarrow e \gamma$ , provides the most stringent bound [2]. The current limit is [3]

$$B(\mu \rightarrow e \gamma) < 1.2 \times 10^{-11} .$$

A proposal is underway, which can improve this limit by three orders of magnitude [4].

In the Lagrangian of the minimal supersymmetric standard model (MSSM), apart from the soft supersymmetry (SUSY) breaking part, there are no lepton-flavor violating terms that would induce lepton-flavor changing processes such as  $\mu \rightarrow e \gamma$ . It is, however, well known that soft SUSY breaking parameters can have all types of flavor-changing terms. Limits on such parameters from  $\mu \rightarrow e \gamma$  have been extensively studied [5]. On the other hand, flavor-changing soft SUSY breaking parameters are often expected to be suppressed by the source of SUSY breaking of a more fundamental theory. A particularly interesting example is the gauge mediation models [6].

Models with “right-handed neutrinos” provide other interesting alternatives with potentially large LFV [7]. It is no surprise that issues of LFV are often tied up with the generation of neutrino masses. Within the MSSM, apart from the soft terms, both LFV and neutrino masses are indeed forbidden by an *ad hoc* discrete symmetry — R parity. Note that the soft terms by themselves still conserve total lepton number, and hence do not generate neutrino masses.

In the supersymmetric standard model without R-parity imposed, there is however another important source of LFV. A major part of this comes simply from the R-parity violating (RPV) terms in the superpotential. We would like to emphasize that the latter is indepen-

dent of SUSY breaking and mediation mechanisms. In fact, the only theoretical means to suppress the flavor-changing effects from RPV couplings would be a generic flavor theory, or some *ad hoc* symmetries such as R-parity itself. Hence, it is important to obtain all the available experimental bounds on the RPV couplings. We show that the experimental limit on the radiative decay of muon,  $\mu \rightarrow e \gamma$ , provides one of the most stringent constraints on the RPV couplings. An improvement of a few orders of magnitude in the experiment may, in fact, discover SUSY as well as the LFV, if the model under consideration does explain the nature.

We first explain a new contribution to the *LR*-slepton mass mixings involving the bilinear  $\mu_i$  and trilinear  $\lambda_{ijk}$  RPV superpotential parameters. Such an important interplay between the bilinear and trilinear couplings was first discussed in Refs. [8,9] in the context of neutrino mass. There is also an analogous contribution to the *LR*-squark mixings, with implications to 1-loop neutrino masses [9] and fermion electric and magnetic dipole moments [10–13]. With nonzero  $\mu_k$  and  $\lambda_{kij}$ , the (off-diagonal) *LR*-mixing involving the  $i, j$  generations is proportional to  $\mu_k^* \lambda_{kij}$  (sum over  $k$ ). With no particular arguments or theories to enforce  $\lambda_{kij}$  to be diagonal in the last two indices, the LFV proportional to  $\mu_k^* \lambda_{kij}$  turns out to be quite natural. The combination  $\mu_k^* \lambda_{kij}$  conserves the overall lepton number but violates lepton flavor. There is another similar contribution to slepton masses in the *LL* mixing part in the form of  $\mu_i^* \mu_j$ . So far as we know, the implication of such terms in the slepton mass matrix is discussed here for the first time. The structure also illustrates very clearly the basics of the LFV structure, which comes into  $\mu \rightarrow e \gamma$ , for example, in other ways too, as we will see below.

In this article, we presented a systematic analysis of the  $\mu \rightarrow e \gamma$  emphasizing the new RPV contributions. We work within the framework of the single-VEV parametrization (SVP) [14,15], which is an optimal choice of flavor basis that helps to guarantee a consistent and unambiguous treatment of all kinds of admissible RPV couplings and to maintain a simple structure for RPV effects on tree-level mass matrices for all states including scalars and fermions [16]. Note that under the SVP, the above-mentioned terms with LFV represent the full RPV contribution to the corresponding entries in the (charged) slepton mass matrix. Obviously, the  $\mu_i^* \mu_j$  combinations contribute equally to the neutral scalar (“sneutrino”)

masses. There are other interesting RPV contributions that mix the sleptons with the other scalars (“Higgses”). Among the latter are the interesting contributions from the soft  $B_i$  parameters. They come into  $\mu \rightarrow e \gamma$  at a different level.

The present work differs from previous ones on the topic [17–21] in a few important ways. Ours is based on the most generic theory of SUSY without R-parity, *i.e.*, no assumptions on the form of R-parity violation, while most of the previous authors worked in various limited RPV scenarios. The only exception is the recent paper of Ref. [20], which basically works under the same framework as ours. They include the *LR*-slepton mixing contribution, following the suggestion of Ref. [10], where the closely related subject of fermion electric dipole moments is discussed. However, the results presented are not as complete and systematic as our treatment here. In particular, there is no discussion of the LFV from the bilinear RPV parameters only. In addition, their bounds on  $\mu_k^* \lambda_{kij}$  have a  $\cos\beta$  dependence, which we disagree with. Other than that, the above new RPV contributions have not been studied before.

The organization of the paper is as follows. In Sec. II, we give the general formulas in the basis of mass eigenstates. The focus is on the  $\ell_j^- \rightarrow \ell_i^- \gamma$  amplitude from 1-loop diagrams without colored intermediate states. Though the small deviations of the external physical charged lepton mass eigenstates ( $\ell_i^\pm$ 's) from the electroweak states  $l_i^\pm$ 's are neglected, full attention is given to such deviations for the particles running in the loop when we analyze the diagrams. Likewise, exact mass eigenstates are always used in the numerical calculations of the 1-loop amplitudes. The formulas can be easily adapted for the radiative  $\tau$  decay with simple substitutions. Guided by the formulas and results from our exact numerical calculation, we analyze in detail the important pieces of 1-loop contributions in Sec. III. Numerical results are presented and discussed in Sec. IV; after which we conclude the article in Sec. V. For the readers who are more interested in the major features of the result, rather than the sophisticated details on how each RPV parameter comes into play in the process, Sec. III can simply be skipped. The section also serves as an analytical confirmation of the correctness of the numerical results, for the more serious readers.

## II. CALCULATION IN MASS BASIS

Here we calculate the decay rate of  $\mu \rightarrow e \gamma$  through colorless 1-loop diagrams using exact mass eigenstates for particles appearing inside the loop. However, as stated above, for the external legs to the loop, we use only electroweak states ( $l_i^\mp$ 's). Each of the latter has a minimal deviation from the corresponding  $L$ - or  $R$ -handed component of the physical charged lepton states as a result of the corresponding small RPV  $\mu_i$  terms [14].

### A. Model background

We work in the framework of the generic supersymmetric standard model [15,22], known as SUSY without R-parity. Here one could simply give up the notion of R-parity; however, the latter terminology is convenient for comparison with the more popular MSSM, as well as other limited studies of R-parity violations. We adopt exactly the same notation as in Refs. [11,15], to which readers are referred for more details. Let us summarize some of the useful notation here, starting from the generic superpotential

$$W = \varepsilon_{ab} \left[ \mu_\alpha \hat{H}_u^a \hat{L}_\alpha^b + y_{ik}^u \hat{Q}_i^a \hat{H}_u^b \hat{U}_k^C + \lambda'_{\alpha jk} \hat{L}_\alpha^a \hat{Q}_j^b \hat{D}_k^C + \frac{1}{2} \lambda_{\alpha \beta k} \hat{L}_\alpha^a \hat{L}_\beta^b \hat{E}_k^C \right] + \frac{1}{2} \lambda''_{ijk} \hat{U}_i^C \hat{D}_j^C \hat{D}_k^C$$

(with  $\alpha, \beta$  going from 0 to 3,  $i, j, k$  from 1 to 3, and  $\epsilon_{12} = -\epsilon_{21} = 1$ ). The essential features of the SVP adopted include  $\langle \hat{L}_i \rangle \equiv 0$  and the identification of  $\hat{L}_0$  as  $\hat{H}_d$ ; related to that is the fact that  $\lambda_{0ii} \equiv y_e$  is the diagonal “leptonic Yukawa” couplings, while  $\lambda_{0ij} \equiv 0$  for  $i \neq j$ .

(i) We have five (color-singlet) charged fermions from  $R$ - and  $L$ -handed mass eigenstates written, respectively, as  $(\chi_{+n}) = \mathbf{V}^T [-i\tilde{W}^+, \tilde{h}_u^+, l_1^+, l_2^+, l_3^+]^T$  and  $(\chi_{-n}) = \mathbf{U}^\dagger [-i\tilde{W}^-, \tilde{l}_0^-, l_1^-, l_2^-, l_3^-]^T$ , where the notation for the electroweak states is quite obvious. So,  $\mathbf{V}^\dagger \mathcal{M}_c \mathbf{U} = \text{diag}\{M_{\chi_n^-}\} \equiv \text{diag}\{M_{c1}, M_{c2}, m_e, m_\mu, m_\tau\}$ . The first two mass eigenvalues are the chargino masses. Note that under the SVP, the only RPV parameters going into the tree level mass matrix  $\mathcal{M}_c$  are the three  $\mu_i$ 's.

(ii) The neutral fermion mass matrix  $\mathcal{M}_N$  is written in the basis  $(-i\tilde{B}, -i\tilde{W}, \tilde{h}_u^0, \tilde{h}_d^0, l_1^0, l_2^0, l_3^0)$ , where  $\tilde{h}_d^0 \equiv l_0^0$ . The symmetric, but generically non-hermitian, mass matrix is diagonalized by a unitary matrix  $\mathbf{X}$  such that  $\mathbf{X}^T \mathcal{M}_N \mathbf{X} = \text{diag}\{M_{\chi_n^0}\}$ , with  $n = 1$  to 4 being the heavy states (neutralinos) and  $n = 5$  to 7 the physical neutrino states at tree-level.

(iii) There are  $1+4+3$  charged scalars that contribute one unphysical Goldstone state after diagonalization. We use the basis  $\{ h_u^{+\dagger}, \tilde{l}_0^-, \tilde{l}_1^-, \tilde{l}_2^-, \tilde{l}_3^-, \tilde{l}_1^{+\dagger}, \tilde{l}_2^{+\dagger}, \tilde{l}_3^{+\dagger} \}$  to write the mass-squared matrix as follows :

$$\mathcal{M}_E^2 = \begin{pmatrix} \tilde{\mathcal{M}}_{Hu}^2 & \tilde{\mathcal{M}}_{LH}^{2\dagger} & \tilde{\mathcal{M}}_{RH}^{2\dagger} \\ \tilde{\mathcal{M}}_{LH}^2 & \tilde{\mathcal{M}}_{LL}^2 & \tilde{\mathcal{M}}_{RL}^{2\dagger} \\ \tilde{\mathcal{M}}_{RH}^2 & \tilde{\mathcal{M}}_{RL}^2 & \tilde{\mathcal{M}}_{RR}^2 \end{pmatrix}; \quad (1)$$

where

$$\begin{aligned} \tilde{\mathcal{M}}_{Hu}^2 &= \tilde{m}_{Hu}^2 + \mu_\alpha^* \mu_\alpha + M_Z^2 \cos 2\beta \left[ \frac{1}{2} - \sin^2 \theta_W \right] \\ &\quad + M_Z^2 \sin^2 \beta [1 - \sin^2 \theta_W], \\ \tilde{\mathcal{M}}_{LL}^2 &= \tilde{m}_L^2 + m_L^\dagger m_L + (\mu_\alpha^* \mu_\beta) + M_Z^2 \cos 2\beta \left[ -\frac{1}{2} + \sin^2 \theta_W \right] 1_{4 \times 4}, \\ &\quad + \begin{pmatrix} M_Z^2 \cos^2 \beta [1 - \sin^2 \theta_W] & 0_{1 \times 3} \\ 0_{3 \times 1} & 0_{3 \times 3} \end{pmatrix}, \\ \tilde{\mathcal{M}}_{RR}^2 &= \tilde{m}_E^2 + m_E m_E^\dagger + M_Z^2 \cos 2\beta [-\sin^2 \theta_W] 1_{3 \times 3}; \end{aligned} \quad (2)$$

and

$$\begin{aligned} \tilde{\mathcal{M}}_{LH}^2 &= (B_\alpha^*) + \begin{pmatrix} \frac{1}{2} M_Z^2 \sin 2\beta [1 - \sin^2 \theta_W] \\ 0_{3 \times 1} \end{pmatrix}, \\ \tilde{\mathcal{M}}_{RH}^2 &= -(\mu_i^* \lambda_{iok}) \frac{v_0}{\sqrt{2}} = (\mu_k^* m_k) \quad (\text{no sum over } k), \\ (\tilde{\mathcal{M}}_{RL}^2)^T &= \begin{pmatrix} 0 \\ A^E \end{pmatrix} \frac{v_0}{\sqrt{2}} - (\mu_\alpha^* \lambda_{\alpha\beta k}) \frac{v_u}{\sqrt{2}} \\ &= [A_e - \mu_0^* \tan \beta] \begin{pmatrix} 0 \\ m_E \end{pmatrix} + \frac{\sqrt{2} M_W \cos \beta}{g_2} \begin{pmatrix} 0 \\ \delta A^E \end{pmatrix} - \begin{pmatrix} -\mu_k^* m_k \tan \beta \\ \frac{\sqrt{2} M_W \sin \beta}{g_2} (\mu_i^* \lambda_{ijk}) \end{pmatrix}. \end{aligned} \quad (3)$$

Introducing the diagonalizing matrix  $\mathcal{D}^l$ , we have  $\mathcal{D}^{l\dagger} \mathcal{M}_E^2 \mathcal{D}^l = \text{diag}\{ M_{\tilde{l}_m}^2, m = 1 \text{ to } 8 \}$ . We label the unphysical Goldstone mode by  $m = 1$ . With relatively small RPV parameters the  $\mathcal{M}_E^2$  is predominantly diagonal, apart from the mixing between the Higgs bosons (*i.e.*,  $h_u$  and  $h_d \equiv \tilde{l}_0$ ) to give the  $m = 1$  mode. The matrix  $\mathcal{D}^l$  may then be naturally organized with all diagonal entries being of order one and only the 12 and 21 entries being possibly large (of order one) among the off-diagonal ones.

(iv) The neutral scalar mass terms, in terms of the  $(1+4)$  complex scalar fields,  $\phi_n$ 's, can be written in two parts — a simple  $(\mathcal{M}_{\phi\phi}^2)_{mn} \phi_m^\dagger \phi_n$  part, and a Majorana-like part in the form  $\frac{1}{2} (\mathcal{M}_{\phi\phi}^2)_{mn} \phi_m \phi_n + \text{h.c.}$ . As the neutral scalars are originated from chiral doublet superfields, the existence of the Majorana-like part is a direct consequence of the electroweak symmetry breaking VEVs, hence restricted to the scalars playing the Higgs role only. They come from the quartic terms of the Higgs fields in the scalar potential. Using the  $\phi_n$  basis  $(h_u^0, \tilde{l}_0^0, \tilde{l}_1^0, \tilde{l}_2^0, \tilde{l}_3^0)$ , we have, explicitly,

$$\mathcal{M}_{\phi\phi}^2 = \frac{1}{2} M_Z^2 \begin{pmatrix} \sin^2\beta & -\cos\beta \sin\beta & 0_{1 \times 3} \\ -\cos\beta \sin\beta & \cos^2\beta & 0_{1 \times 3} \\ 0_{3 \times 1} & 0_{3 \times 1} & 0_{3 \times 3} \end{pmatrix}; \quad (4)$$

and

$$\mathcal{M}_{\phi\phi^\dagger}^2 = \begin{pmatrix} \tilde{m}_{H_u}^2 + \mu_\alpha^* \mu_\alpha + M_Z^2 \cos 2\beta \left[ -\frac{1}{2} \right] & -(B_\alpha) \\ -(B_\alpha^*) & \tilde{m}_L^2 + (\mu_\alpha^* \mu_\beta) + M_Z^2 \cos 2\beta \left[ \frac{1}{2} \right] \end{pmatrix} + \mathcal{M}_{\phi\phi}^2. \quad (5)$$

Note that  $\mathcal{M}_{\phi\phi}^2$  here is real (see Appendix A of Ref. [9]), while  $\mathcal{M}_{\phi\phi^\dagger}^2$  does have complex entries. Writing the five  $\phi_n$ 's in terms of their scalar and pseudoscalar parts, the full  $10 \times 10$  (real and symmetric) mass-squared matrix for the real scalars is then given by

$$\mathcal{M}_s^2 = \begin{pmatrix} \mathcal{M}_{ss}^2 & \mathcal{M}_{sp}^2 \\ (\mathcal{M}_{sp}^2)^T & \mathcal{M}_{pp}^2 \end{pmatrix}, \quad (6)$$

where the scalar, pseudoscalar, and mixing parts are

$$\begin{aligned} \mathcal{M}_{ss}^2 &= \text{Re}(\mathcal{M}_{\phi\phi^\dagger}^2) + \mathcal{M}_{\phi\phi}^2, \\ \mathcal{M}_{pp}^2 &= \text{Re}(\mathcal{M}_{\phi\phi^\dagger}^2) - \mathcal{M}_{\phi\phi}^2, \\ \mathcal{M}_{sp}^2 &= -\text{Im}(\mathcal{M}_{\phi\phi^\dagger}^2), \end{aligned} \quad (7)$$

respectively. If  $\text{Im}(\mathcal{M}_{\phi\phi^\dagger}^2)$  vanishes, the scalars and pseudoscalars decouple from one another and the unphysical Goldstone mode would be found among the latter. Note that the  $B_\alpha$  entries may also be considered as a kind of  $LR$  mixings.

As a real scalar mass matrix,  $\mathcal{M}_s^2$  could be diagonalized by an orthogonal matrix  $\mathcal{D}^s$ . However, we will write  $\mathcal{D}^s$  as if it is just a unitary matrix. This would be useful for illustrating

some theoretical features in the discussions below. In fact, it helps sometimes to think about the neutral scalars as complex scalars instead of in terms of the scalar and pseudoscalar constituents. This is especially true for the “sneutrino” parts. Hence, we write  $\mathcal{D}^{s\dagger} \mathcal{M}_s^2 \mathcal{D}^s = \text{diag}\{M_{s_m}^2, m = 1 \text{ to } 10\}$ . Again, it is useful to consider the form of  $\mathcal{D}^s$  very close to the identity matrix, *i.e.*, with all diagonal entries being of order one. The unphysical Goldstone mode has, of course, to be found mainly among the first two pseudoscalars. The mode is naturally labeled as the  $m = 6$  mass eigenstate here. Similar to the previous case, all the off-diagonal entries, except those related to mixing of the Higgs bosons (*i.e.*, the 12, 21, 67, and 76 entries) are expected to be relatively small.

(v) In the diagonalization of the neutral- and charged-scalar mass-squared matrices given above, one has to impose all the proper tadpole conditions to get the correct unphysical Goldstone modes explicitly. Under the SVP, the tadpole conditions are (see Appendix A of Ref. [9] for more details)

$$B_0 \cot\beta = \left[ \tilde{m}_{H_u}^2 + \mu_\alpha^* \mu_\alpha + \frac{1}{8}(g_1^2 + g_2^2)(v_u^2 - v_d^2) \right], \quad (8)$$

$$B_0 \tan\beta = \left[ \tilde{m}_{L_{00}}^2 + |\mu_0|^2 + \frac{1}{8}(g_1^2 + g_2^2)(v_d^2 - v_u^2) \right], \quad (9)$$

$$B_i \tan\beta = \tilde{m}_{L_{0i}}^2 + \mu_0^* \mu_i \quad (i = 1, 2, 3). \quad (10)$$

The last equation represents the redundancy in parameters explicitly identified under the optimal parametrization (SVP) used. Hence, within the formulation, the RPV parameters  $B_i$ 's and  $\mu_i$ 's are not exactly independent quantities. Here, the  $\tilde{m}_{L_{0i}}^2$ 's play an interesting role very different from the R-parity conserving elements  $\tilde{m}_{L_{ij}}^2$ 's in the same matrix. What values the  $\tilde{m}_{L_{0i}}^2$ 's might naturally take is quite a technical issue. While the off-diagonal  $\tilde{m}_{L_{ij}}^2$ 's characterize LFV from soft SUSY breaking, the  $\tilde{m}_{L_{0i}}^2$ 's could be so interpreted only when the SUSY breaking mechanism naturally gives vanishing VEV's for the  $\hat{L}_i$ 's. Such a scenario is indeed possible [23]. In a more generic situation, one can still think about taking the low-energy Lagrangian and perform the necessary rotation to recast the model into the SVP framework. Such a rotation may generate nonzero  $\tilde{m}_{L_{0i}}^2$ 's to guarantee the satisfaction of Eq.(10) in the new basis. Hence, when we switch off the  $\tilde{m}_{L_{ij}}^2$ 's to single out the RPV contributions to LFV below, the  $\tilde{m}_{L_{0i}}^2$ 's will not be handled in the same fashion. We will discuss more the implications of Eq.(10) in relation to  $\mu \rightarrow e\gamma$  below. We emphasize here

again that the above tadpole conditions are very important and should not be overlooked in any discussion of the phenomenology, particularly those related to the  $B_i$ 's.

### B. The $\ell_j^- \rightarrow \ell_i^- \gamma$ amplitude from (colorless) 1-loop diagrams

Once we have the above matrices we can express the effective interactions involving an external charged lepton with internal particles in terms of the mass eigenstates and the elements of diagonalizing matrices. The effective interaction for an external charged lepton, taken as an  $l_i^-$  or  $l_i^+$  state for the  $L$ - or  $R$ -handed component here, with exact physical charged scalars and neutral fermions inside the loop is given by

$$\mathcal{L} = g_2 \bar{\Psi}(l_i) \left[ \mathcal{N}_{inm}^L \frac{1 - \gamma_5}{2} + \mathcal{N}_{inm}^R \frac{1 + \gamma_5}{2} \right] \Psi(\chi_n^0) \phi_m^- + \text{h.c.} , \quad (11)$$

where  $\frac{1}{2}(1 \mp \gamma_5)$  are the  $L$ - and  $R$ -handed projections and

$$\mathcal{N}_{inm}^R = \frac{1}{\sqrt{2}} [\tan \theta_W \mathbf{X}_{1n}^* + \mathbf{X}_{2n}^*] \mathcal{D}_{(i+2)m}^l - \frac{y_{e_i}}{g_2} \mathbf{X}_{4n}^* \mathcal{D}_{(i+5)m}^l - \frac{\lambda_{khi}^*}{g_2} \mathbf{X}_{(k+4)n}^* \mathcal{D}_{(h+5)m}^l , \quad (12)$$

$$\mathcal{N}_{inm}^L = -\sqrt{2} \tan \theta_W \mathbf{X}_{1n} \mathcal{D}_{(i+5)m}^l - \frac{y_{e_i}}{g_2} \mathbf{X}_{4n} \mathcal{D}_{(i+2)m}^l + \frac{y_{e_i}}{g_2} \mathbf{X}_{(i+4)n} \mathcal{D}_{2m}^l - \frac{\lambda_{khi}}{g_2} \mathbf{X}_{(k+4)n} \mathcal{D}_{(h+2)m}^l , \quad (13)$$

with  $n$  runs from 1 to 7 and  $m$  from 1 to 8. We called this class of contributions neutralino-like, which obviously does include the ones with the physical neutralinos among the most important parts. The terms in  $\mathcal{N}_{inm}^{L,R}$  are easy to understand. For example, in  $\mathcal{N}_{inm}^R$ , the first two terms denote the interactions with  $L$ -handed sleptons and the bino and wino, respectively. The third term is the interaction with  $R$ -handed sleptons and the higgsino, while the fourth term describes the interaction with  $R$ -handed sleptons and the neutrino flavor states. Next, we come to the chargino-like contributions. The corresponding effective interaction for the external charged lepton  $l_i^\mp$  with exact physical neutral scalars and charged fermions inside the loop is given by

$$\mathcal{L} = g_2 \bar{\Psi}(l_i) \left[ \mathcal{C}_{inm}^L \frac{1 - \gamma_5}{2} + \mathcal{C}_{inm}^R \frac{1 + \gamma_5}{2} \right] \Psi(\chi_n^-) \phi_m^0 + \text{h.c.} , \quad (14)$$

where

$$\mathcal{C}_{inm}^R = -\mathbf{V}_{1n} \frac{1}{\sqrt{2}} [\mathcal{D}_{(i+2)m}^s + i \mathcal{D}_{(i+7)m}^s] - \frac{y_{e_i}}{g_2} \mathbf{V}_{(i+2)n} \frac{1}{\sqrt{2}} [\mathcal{D}_{2m}^{s*} - i \mathcal{D}_{7m}^{s*}]$$

$$-\frac{\lambda_{hik}^*}{g_2} \mathbf{V}_{(k+2)n} \frac{1}{\sqrt{2}} [\mathcal{D}_{(h+2)m}^{s*} - i \mathcal{D}_{(h+7)m}^{s*}] , \quad (15)$$

$$\begin{aligned} \mathcal{C}_{inm}^L &= \frac{y_{e_i}}{g_2} \mathbf{U}_{2n} \frac{1}{\sqrt{2}} [\mathcal{D}_{(i+2)m}^s + i \mathcal{D}_{(i+7)m}^s] - \frac{y_{e_i}}{g_2} \mathbf{U}_{(i+2)n} \frac{1}{\sqrt{2}} [\mathcal{D}_{2m}^s + i \mathcal{D}_{7m}^s] \\ &\quad + \frac{\lambda_{khi}}{g_2} \mathbf{U}_{(k+2)n} \frac{1}{\sqrt{2}} [\mathcal{D}_{(h+2)m}^s + i \mathcal{D}_{(h+7)m}^s] . \end{aligned} \quad (16)$$

Recall that  $\mathcal{D}^s$  is actually real, though we are using  $\mathcal{D}^{s*}$  notation as if it is not. This is just a convention for tracing the LFV structure of the various contributions in our analytical discussions below. Here, in fact, the real difference between the  $\mathcal{D}^{s*}$  and  $\mathcal{D}^s$  terms is given explicitly by the different signs between the corresponding scalar and pseudoscalar parts. Note that the  $y_{e_i}$  terms in the above expressions can be written together with the  $\lambda$  terms using the  $\lambda_{\alpha\beta k}$  notation and the identification of  $y_{e_i}$  as  $\lambda_{0ii}$ . This common structure between  $\hat{L}_0$  and the  $\hat{L}_i$ 's is very useful in our discussions below.

In applying the above interactions to the process  $\ell_j^-(p) \rightarrow \ell_i^-\gamma(q)$ , we can write the amplitude as

$$T = e \epsilon^{*\alpha} \bar{u}_i(p-q) \left[ m_{\ell_j} i \sigma_{\alpha\beta} q^\beta \left( A_2^L \frac{1-\gamma_5}{2} + A_2^R \frac{1+\gamma_5}{2} \right) \right] u_j(p) , \quad (17)$$

where  $\epsilon^* = \epsilon^*(q)$  is the polarization four vector of the outgoing photon. The decay rate is then simply given by

$$\Gamma(\ell_2^- \rightarrow \ell_1^- \gamma) = \frac{\alpha_{\text{em}}}{4} m_\mu^5 \left( |A_2^L|^2 + |A_2^R|^2 \right) . \quad (18)$$

It is straightforward to calculate the contributions from 1-loop diagrams with the effective interactions of Eqs. (11) and (14). The result for  $A_2^L$  ( $A_2^R = A_2^L|_{L \leftrightarrow R}$ ) is given by

$$\begin{aligned} A_2^L &= \frac{\alpha_{\text{em}}}{8\pi \sin^2 \theta_W} \frac{1}{M_{\ell_m}^2} \left[ \mathcal{N}_{inm}^L \mathcal{N}_{jnm}^{L*} F_2 \left( \frac{M_{\chi_n}^2}{M_{\ell_m}^2} \right) + \mathcal{N}_{inm}^R \mathcal{N}_{jnm}^{R*} \frac{m_{\ell_i}}{m_{\ell_j}} F_2 \left( \frac{M_{\chi_n}^2}{M_{\ell_m}^2} \right) + \mathcal{N}_{inm}^L \mathcal{N}_{jnm}^{R*} \frac{M_{\chi_0}}{m_{\ell_j}} F_3 \left( \frac{M_{\chi_0}^2}{M_{\ell_m}^2} \right) \right] \\ &\quad - \frac{\alpha_{\text{em}}}{8\pi \sin^2 \theta_W} \frac{1}{M_{S_m}^2} \left[ \mathcal{C}_{inm}^L \mathcal{C}_{jnm}^{L*} F_5 \left( \frac{M_{\chi_n}^2}{M_{S_m}^2} \right) + \mathcal{C}_{inm}^R \mathcal{C}_{jnm}^{R*} \frac{m_{\ell_i}}{m_{\ell_j}} F_5 \left( \frac{M_{\chi_n}^2}{M_{S_m}^2} \right) + \mathcal{C}_{inm}^L \mathcal{C}_{jnm}^{R*} \frac{M_{\chi_0}}{m_{\ell_j}} F_6 \left( \frac{M_{\chi_0}^2}{M_{S_m}^2} \right) \right] , \end{aligned} \quad (19)$$

where

$$\begin{aligned} F_2(x) &= \frac{1}{6(1-x)^4} (1 - 6x + 3x^2 + 2x^3 - 6x^2 \ln x) , \\ F_3(x) &= \frac{1}{(1-x)^3} (1 - x^2 + 2x \ln x) , \\ F_5(x) &= \frac{1}{6(1-x)^4} (2 + 3x - 6x^2 + x^3 + 6x \ln x) , \\ F_6(x) &= \frac{1}{(1-x)^3} (-3 + 4x - x^2 - 2 \ln x) , \end{aligned}$$

with summations over all physical fermion and scalar mass eigenstates as represented by the  $n$  and  $m$  indices assumed. Apart from the model being different, our background notation here, such as the loop integral functions, follows mostly that of Ref. [24], to which readers are referred for a comparison.

### III. ANALYSIS OF THE VARIOUS CONTRIBUTIONS

Comparing  $\mathcal{C}^{L,R}$  and  $\mathcal{N}^{L,R}$ , we see that the two types of loop contributions as given in Eq.(19) do have very similar structures. The first type, corresponding to diagrams with a charged fermion and neutral scalar in the loop, are, however, typically larger than their  $SU(2)$  counterparts, *i.e.*, from diagrams with neutral fermions and charged scalars. Hence, we focus our discussions on the  $\mathcal{C}^{L,R}$  part, the chargino-like loop. Before going into the analysis, it is instructive to introduce the lepton-flavor numbers  $L_e$ ,  $L_\mu$ , and  $L_\tau$  to the superfields as one does to their corresponding components in the SM. Some of the RPV parameters would then bear violations of the lepton-flavor numbers. It is obvious that in order to have a contribution to  $\mu^- \rightarrow e^- \gamma$ , a term must reduce  $L_\mu$  and increase  $L_e$  by exactly one unit while leaving  $L_\tau$  unchanged. This simple but useful rule serves as a countercheck of individual contributions discussed below.

The following discussions are concerned with sophisticated analytical details on the more interesting individual pieces of contributions. The aim is to understand the exact role played by each of the RPV parameters in the process, and the strength of each contribution. Reading the section would take a bit of effort, which is not necessary for a general reader interested mainly in knowing the basic features of the results. While we will refer to some analytical results presented here in the discussion of the numerical results in the next section, for comparison and confirmation, a general reader may simply skip this section.

#### A. Chirality flip inside the loop

Take  $A_2^L$ , for example, among the three terms in Eq.(19), the one with  $\mathcal{C}_{1nm}^L \mathcal{C}_{2nm}^{R*}$  corresponds to the diagrams with the chirality flip on the internal fermion line. Hence, the diagrams with the two chargino states (*i.e.*,  $n = 1, 2$ ) would potentially dominate over the

other diagrams with external chirality-flipping mass insertion ( $m_\mu$  or  $m_e$ ).

We first look at the contributions with a  $(\mu^* \lambda)$  structure. Taking only one  $\lambda$ -coupling vertex, one can then take the gauge coupling term (first term) from  $\mathcal{C}_{2nm}^{R*}$ . We then have the real scalar part of the contribution proportional to

$$\sum_{n=1}^5 \sum_{m=1}^5 \mathbf{V}_{1n}^* M_{\chi_n^-} \mathbf{U}_{(k+2)n} F_6 \left( \frac{M_{\chi_n^-}^2}{M_{S_m}^2} \right) \mathcal{D}_{4m}^{s*} \mathcal{D}_{(h+2)m}^s \frac{\lambda_{kh1}}{g_2} . \quad (20)$$

Here we have dropped the pseudoscalar part just for simplicity in this discussion. This is exactly valid when there is no mixings between scalars and pseudoscalars. However, we find it more transparent in illustrating the basic features. If the loop function  $F_6$  could be factored out from the double summation, we would have a  $\mathbf{V}_{1n}^* M_{\chi_n^-} \mathbf{U}_{(k+2)n}$  summation over fermions and a  $\mathcal{D}_{4m}^{s*} \mathcal{D}_{(h+2)m}^s$  summation over (real) scalars. However, the fermionic sum gives exactly the  $l_k^- - \tilde{W}^+$  mass term, which is zero. This is well illustrated by the loop diagram with electroweak state notation, as given in Fig. 1. Hence, one expects a GIM-like cancellation mechanism, here violated only to the extent that  $F_6$  is not universal. The violation is, however, quite substantial, as illustrated in the similar case of quark electric dipole moments [11] and by our exact numerical calculation here. The case of degenerate charginos is an obvious exception, which, however, needs too large a complex phase for  $\mu_0$  to be phenomenologically viable. A similar situation goes with the scalar sum —  $\mathcal{D}_{4m}^{s*} \mathcal{D}_{(h+2)m}^s = \delta_{h2}$  by unitarity. Taking  $h = 2$  in the above expression (20), we have the two dominating chargino contributions, the  $n = 1$  and 2 parts, given approximately by

$$\mathbf{V}_{1n}^* \mu_k^* R_{R_{2n}} \frac{\lambda_{k21}}{g_2} F_6 \left( \frac{M_{\chi_n^-}^2}{M_{S_m}^2} \right) ; \quad (21)$$

where  $R_R$  is a  $2 \times 2$  matrix with order one matrix elements and is the  $R$ -handed transformation needed to diagonalize the  $2 \times 2$  MSSM chargino block (see Appendix A of Ref. [11] for details.) The expected combination  $\mu_k^* \lambda_{k21}$  comes up, with  $k = 1$  and 3 admissible. There is only a partial cancellation between the two parts in general. The same situation goes for the  $\mathcal{C}_{1nm}^R \mathcal{C}_{2nm}^{L*}$  part of  $A_2^R$ , with the combination  $\mu_k \lambda_{k12}^*$  ( $k = 2$  and 3 admissible here) instead. An interesting point to note is that the above expression shows no obvious dependence on  $\tan\beta$ , a result confirmed by our exact numerical calculation. This is an important issue that we will get back to below.

Next, we consider the above expression (20) with  $h \neq 2$ . Let us try to estimate the individual terms in the  $\mathcal{D}_{4m}^{s*} \mathcal{D}_{(h+2)m}^s$  summation. From the structure of the neutral scalar mass matrix, we see that  $\mathcal{M}_{SS}^2$  in particular, is very likely to be predominantly diagonal. Off-diagonal elements in the  $\mathcal{D}^s$  matrix then measure the small mixings. The largest terms among the different  $m$ 's are then given by  $m = 4$  or  $m = h + 2$  with a suppression factor of magnitude  $\mathcal{D}_{(h+2)4}^s = \mathcal{D}_{4(h+2)}^{s*} \sim \frac{\mu_2 \mu_h^*}{\tilde{m}_{L_{hh}}^2 - \tilde{m}_{L_{22}}^2}$ . This result is an example of the  $L$ -slepton flavor mixing from the coupling of the form  $\mu_i^* \mu_j$  mentioned in the Introduction — something that is also useful for our discussion below. The flavor mixing is explicitly given in Eq.(5), in the discussion of the scalar masses, where we explain the notation  $\mathcal{D}^{s*}$  despite its being real. As the RPV mixings are the same in the scalar and pseudoscalar parts ( $\mathcal{M}_{SS}^2$  and  $\mathcal{M}_{PP}^2$ ), one could think in terms of complex scalars here, in which case the complex  $\mathcal{D}^s$  notation would be exactly valid. With a first-order difference between  $\tilde{m}_{L_{hh}}^2$  and  $\tilde{m}_{L_{22}}^2$ , the nonuniversal  $F_6$  function still induce large violation in the unitarity cancellation, essentially between the  $m = 4$  and  $m = h + 2$  parts. For the case at hand, the contribution goes with four, instead of two, RPV parameters (the two combinations  $\mu_2 \mu_h^*$  and  $\mu_k^* \lambda_{kh1}$ ); hence, it is very likely to be subdominating.

There are analogous neutralino-like contributions. However, in the latter case, there is also an extra pure gaugino loop, from the first terms in Eqs.(12) and (13) with no parallel chargino-like counterparts. This contribution involves  $\mathcal{D}_{4m}^{l*} \mathcal{D}_{6m}^l$  or  $\mathcal{D}_{7m}^{l*} \mathcal{D}_{3m}^l$ , hence a  $LR$ -slepton mixing, with RPV contribution given by  $\mu_k^* \lambda_{k21}$  or  $\mu_k \lambda_{k12}^*$  (for  $A_2^L$  or  $A_2^R$ , respectively). This is the most intuitive contribution involving the combination of parameters that we mentioned in the introduction. Numerically, this contribution is, typically, only similar to other neutralino-like terms with one gauge coupling vertex, and hence smaller than the dominating chargino-like term discussed above. The reason here is that the larger gauge coupling effect is offset by the suppression factor coming from the  $LR$ -mixing. However, if one pushes for a large  $|\mu_0|$  value while keeping the bino mass  $M_1$  small, the other contributions, including the whole chargino-like loop contribution could become suppressed, thus leaving the pure gauge loop to be the dominating one.

Replacing the  $\lambda$  coupling in the above contributions [*cf.* expression (20)] with a “leptonic Yukawa coupling” (recall  $y_{ei} \equiv \lambda_{0ii}$ ), we have a

$$\sum_{n=1}^5 \sum_{m=1}^5 \mathbf{V}_{1n}^* M_{\chi_n^-} \mathbf{U}_{2n} F_6 \left( \frac{M_{\chi_n^-}^2}{M_{S_m}^2} \right) \mathcal{D}_{4m}^{s*} \mathcal{D}_{3m}^s \frac{y_{e_1}}{g_2} \quad (22)$$

part. Here, the fermionic sum has obviously a dominating chargino contribution without the need for RPV parameters. However, we have no choice but the fixed scalar mixings given by  $\mathcal{D}_{4m}^{s*} \mathcal{D}_{3m}^s$ . As discussed above, the latter involves  $\mu_1^* \mu_2$ . With the small  $y_{e_1}$  coupling, it gives a strong suppression. Of course the “electron Yukawa”  $y_{e_1}$  above can be exchanged for the larger “muon Yukawa”  $y_{e_2}$  in the corresponding piece in  $A_2^R$  instead. The latter give the same  $\mathcal{D}_{4m}^{s*} \mathcal{D}_{3m}^s$  scalar mixing factor. This contribution is depicted in Fig. 2.

From Eqs.(15) and (16), there is one more similar but independent term. This has expression (22) modified with a simple switching of the explicit 2 and 3 indices, and a sign flip. Here we write down explicitly the corresponding term from  $A_2^R$  instead :

$$\sum_{n=1}^5 \sum_{m=1}^5 -\mathbf{V}_{1n} M_{\chi_n^-} \mathbf{U}_{4n}^* F_6 \left( \frac{M_{\chi_n^-}^2}{M_{S_m}^2} \right) \mathcal{D}_{3m}^s \mathcal{D}_{2m}^{s*} \frac{y_{e_2}}{g_2} . \quad (23)$$

From the above discussion, it is easy to see that the dominating part with the charginos ( $n = 1$  and 2) gives a  $\mu_2$  dependence through  $\mathbf{U}_{4n}^*$ . Naively, we expect a  $\mu_1^*$  from the scalar mixing part. The mixing of the corresponding complex scalars, however, involves a 32-entry of the  $\mathcal{M}_{\phi\phi}^2$  matrix. From the result given in the Sec. IIA, we see that the mixing does have a  $\mu_1^*$ . But it comes in the combination  $\tilde{m}_{L_{10}}^2 + \mu_1^* \mu_0$ . The latter is, by the tadpole equation (10),  $B_1^* \tan\beta$ . Detailed analysis of the full scalar mass matrix, with the first-order mixings among the Higgs states, does not change the  $B_1^* \tan\beta$  dependence of the result. Hence, the LFV structure here is given by the RPV parameter combination  $B_1^* \mu_2$ , which is related to the  $\mu_1^* \mu_2$  combination through the tadpole equation. Given in terms of  $B_1^*$ , the contribution has an explicit  $\tan\beta$  dependence. In general, one expects this contribution to be of comparable magnitude to the previous one.

The last contribution we want to discuss here is the one with two  $\lambda$  couplings. Extracting the part similar to expression (20), we have

$$\sum_m' \sum_{n=1}^5 \mathbf{V}_{(k'+2)n}^* M_{\chi_n^-} \mathbf{U}_{(k+2)n} F_6 \left( \frac{M_{\chi_n^-}^2}{M_{S_m}^2} \right) [\mathcal{D}_{(h'+2)m}^s + i\mathcal{D}_{(h'+7)m}^s] [\mathcal{D}_{(h+2)m}^s + i\mathcal{D}_{(h+7)m}^s] \frac{\lambda_{h'2k'}}{g_2} \frac{\lambda_{kh1}}{g_2} . \quad (24)$$

Note that we have written the expression very differently here. Both the scalar and pseudoscalar parts are explicitly shown. The sum over  $m$ , scalar mass eigenstates, goes over all

nine physical states (the  $\Sigma'_m$  notation means the unphysical Goldstone mode is omitted). The interesting point here is that this contribution involves a nontrivial interplay between two parts. A careful reading of the  $\lambda_{h'2k'}^*$  term in Eq.(15) would appreciate that the scalar mixing matrix comes in as  $\mathcal{D}^{s*}$  instead, or, equivalently, the scalar and pseudoscalar parts come in with the “wrong” sign. At the limit of degenerate but unmixed scalars and pseudoscalars, the “right” signs (or with  $\mathcal{D}^s$ , as in the case of the first gauge coupling term) would give identical contributions from the two parts; while the “wrong” signs would give an exact cancellation instead. To put it in another way, a Majorana-like scalar mass insertion along the scalar line is needed to have the contribution nonzero, as depicted in Fig. 3. There have been some discussions on the Majorana-like scalar mass terms for the “sneutrinos” (or  $\tilde{l}_i^0$  states to be exact) as complex scalars, and some of the resulting phenomenological implications are studied in recent literature [25,26]. Such mass terms appear under the SVP through LFV from the soft  $B_i$  parameters. An illustration of the Majorana-like scalar mass terms is shown explicitly in Fig. 3b. It can be easily seen that the contribution under discussion here actually involves a minimum of four RPV parameters,  $B_{h'}^* B_h^*$  and  $\lambda_{h'2k'} \lambda_{kh_1}$ , and it is achieved by taking  $k = k'$ . An interesting point, at least from the theoretical point of view, is that the contribution could have a different flavor structure from the more familiar two- $\lambda$  loop diagrams with the chirality flip on the external muon line [19], and a  $m_\tau$  instead of  $m_\mu$  dependence too. For instance, we could have a new contribution from the  $\lambda_{123} \lambda_{311}$  combination.

Finally, we want to remark that the remaining contributions with internal chirality flip can be analyzed again by using the extended flavor structure with the “leptonic Yukawa coupling”  $y_{e_i}$  identified as  $\lambda_{0ii}$ , as discussed above. In fact, Fig. 3a is given with the generic  $\lambda_{\alpha\beta k}$  notation and hence applicable to this latter case. One can obtain contributions depending only on a  $B_h^*$  and  $\lambda_{h21}$  combination, for example. Explicitly, we have expression (24) modified to

$$\sum_m' \sum_{n=1}^5 \mathbf{V}_{4n}^* M_{\chi_n} \mathbf{U}_{4n} F_6 \left( \frac{M_{\chi_n}^2}{M_{S_m}^2} \right) [\mathcal{D}_{2m}^s + i\mathcal{D}_{7m}^s] [\mathcal{D}_{(h+2)m}^s + i\mathcal{D}_{(h+7)m}^s] \frac{y_{e_2}}{g_2} \frac{-\lambda_{h21}}{g_2}, \quad (25)$$

with which the fermionic sum suggests a major contribution from  $n = 4$ , *i.e.*, the muon itself with the  $m_\mu$  dependence, and the scalar sum gives the dominating contribution proportional to  $B_h^*$ . However, this contribution then has two factors of “muon Yukawa” ( $y_{e_2}$ ) suppression.

Hence, it is not a very important contribution. Note that the Majorana-like scalar mass required can be interpreted as in the same form as given by Fig. 3b, with a  $B_0^*$  and a  $B_h^*$ , except that the  $B_0^*$  insertion, in general, has no suppression; the  $B_0^*$  is actually not necessary to complete the corresponding diagram in Fig. 3a in this case though, due to the existence of the  $\hat{L}_0$  (or, equivalently  $\tilde{l}_0 \equiv h_d$ ) VEV.

### B. Chirality flip on the external muon line

Contributions from the terms with the chirality flip on the external muon line is expected to be suppressed by a  $y_{e_2}$  ( $\sim 10^{-3}$ ) factor. However, we have seen that apart from the  $\mu^* \lambda$ -type combination, other combinations of RPV parameters that come into the diagrams with an internal chirality flip do have extra suppressions. Hence, it is still of interest to see if there are important terms with an external chirality flip that are comparable to those discussed in the previous section. Therefore, we mainly look for terms depending on only two RPV parameters without further extra suppressions, apart from the one dictated by the chirality flip.

For the chargino-like diagrams, for instance, our candidates here are from the  $\mathcal{C}_{1nm}^L \mathcal{C}_{2nm}^{L*}$  part of  $A_2^L$  and the  $\mathcal{C}_{1nm}^R \mathcal{C}_{2nm}^{R*}$  part of  $A_2^R$ . The latter looks more interesting. First of all, there is a pure gauge loop, as shown in Fig. 4a. Compared with the above, we have the analogous expression

$$m_\mu \sum_{n=1}^5 \sum_{m=1}^5 -\mathbf{V}_{1n}^* \mathbf{V}_{1n} F_5\left(\frac{M_{\chi_n}^2}{M_{S_m}^2}\right) \mathcal{D}_{4m}^{s*} \mathcal{D}_{3m}^s. \quad (26)$$

The scalar mixing part gives the  $\mu_1^* \mu_2$  LFV structure. This looks comparable with expression (22).

The only other term from  $\mathcal{C}_{1nm}^R \mathcal{C}_{2nm}^{R*}$  without further  $y_{e_i}$  suppression is the usual 2- $\lambda$  term discussed much earlier in the literature, together with similar (colored) 2- $\lambda$  diagrams [19]. We have an expression given by

$$m_\mu \sum_{n=1}^5 \sum_{m=1}^5 -\mathbf{V}_{(k'+2)n}^* \mathbf{V}_{(k+2)n} F_5\left(\frac{M_{\chi_n}^2}{M_{S_m}^2}\right) \mathcal{D}_{(h'+2)m}^s \mathcal{D}_{(h+2)m}^{s*} \frac{\lambda_{h'2k'}}{g_2} \frac{\lambda_{h1k}^*}{g_2}, \quad (27)$$

requiring further  $h = h'$  and  $k = k'$ . Note that all off-diagonal matrix elements of the form  $\mathbf{V}_{(k+2)n}$  are very small, those RPV ones ( $n = 1$  or  $2$ ) in particular further contain a

$y_{e_i}$  suppression (see Appendix A of Ref. [11]). Finally, with the  $\mathcal{C}_{1nm}^L \mathcal{C}_{2nm}^{L*}$  part of  $A_2^L$ , we are obviously left only with the other  $2\lambda$  terms [19].

The neutralino-like loop contributions are mostly straight forward analogs, except for the contributions with only one gauge coupling. Unlike the chargino-like case discussed above, there may be no extra  $y_{e_i}$  suppression, from a  $\mathbf{V}$  element or otherwise. However, an extra  $LR$ -mixing is involved, giving another suppression, as illustrated in Fig. 4b.

The only relatively important type of contributions involving the combination such as  $B_h^* \lambda_{h21}$  has two factors of  $y_{e_2}$  suppression. If one is interesting in the dominating contribution of this type, an external chirality flip term with only one extra  $y_{e_2}$  suppression may have to be considered. In fact, such a contribution does exist. The  $\mathcal{C}_{1nm}^L \mathcal{C}_{2nm}^{L*}$  part of  $A_2^L$  has a piece of the form

$$m_\mu \sum_{n=1}^5 \sum_{m=1}^5 -\mathbf{U}_{4n}^* \mathbf{U}_{4n} F_5 \left( \frac{M_{\chi_n^-}^2}{M_{S_m}^2} \right) \mathcal{D}_{(h+2)m}^s \mathcal{D}_{2m}^{s*} \frac{-\lambda_{h21}}{g_2} \frac{-y_{e_2}}{g_2}, \quad (28)$$

where we have  $h = 3$  or  $1$ . This is expected to be of similar strength to the one in expression (25) discussed above. Recall that the scalar mixings give a  $B_h^* \tan\beta$  dependence.

#### IV. EXACT NUMERICAL CALCULATIONS AND RESULTS

In this section, we present the results we obtained by a careful numerical implementation of our  $\mu \rightarrow e \gamma$  formulas, with explicit numerical diagonalization of all the mass matrices involved. We isolate various major contributions by singling out each of the corresponding RPV parameter combinations as the only nonvanishing ones. The soft SUSY breaking contributions to R-parity conserving slepton mixings are set to zero (*i.e.*,  $\tilde{m}_L^2$ ,  $\tilde{m}_E^2$ , and  $A^E$  are set to be diagonal). Though we have used only real numbers for all input parameters in the numerical results presented, our discussions apply to the general case of complex parameters, as does the analysis given above. A basic set of typical values chosen for the input parameters are given in Table I. We used this set of inputs unless otherwise specified in the results below. At the end, we also show the effects of varying these input parameters.

At the beginning of the previous section, we introduced a useful rule in terms of lepton-flavor number violation counts; *i.e.*, an admissible contribution has to include RPV parameters such that it reduces  $L_\mu$  and increases  $L_e$  by exactly one unit while leaving  $L_\tau$

untouched. Moreover,  $\mu \rightarrow e \gamma$  is an R-parity even process. The rule alone can be used to identify a few interesting cases of two RPV parameter combinations. We first concentrate on the superpotential parameters. Using the bilinear parameters, we have only the  $\mu_1^* \mu_2$  combination. With the trilinear parameters, there are various  $2\text{-}\lambda$  and  $2\text{-}\lambda'$  combinations. Such contributions to  $\mu \rightarrow e \gamma$  are well studied [19]. It is easy to see that as the  $\lambda'$  couplings involve quarks and squarks while the others do not, there is no combination of a single  $\lambda'$  with a coupling of the other types contributing to 1-loop  $\mu \rightarrow e \gamma$ . We skip the quark-squark loop contributions here. The  $2\text{-}\lambda$  loops, however, is an integral part of our (colorless loop) formulas. We will discuss such contributions also for completeness and for easy comparison with previous works. Most interestingly, however, are the combinations involving RPV parameters of both the bilinear and trilinear types. They are  $\mu_k^* \lambda_{k21}$  with  $k$  being 3 or 1, and  $\mu_k \lambda_{k12}^*$  with  $k$  being 3 or 2.

Next, we add into consideration the RPV parameters from soft SUSY breaking. The trilinear  $A^\lambda$  terms have no role to play here, because under the SVP such terms give only three-scalar interaction vertices, which obviously cannot be incorporated into any 1-loop  $\mu \rightarrow e \gamma$  diagram. This leaves the  $B_i$ 's and  $\tilde{m}_{L0i}^2$ 's. However, as commented above in the last part of Sec. IIA, we have the important tadpole conditions in Eq.(10) relating these two sets of parameters to the  $\mu_i$ 's. In the literature,  $\mu_i$ 's and  $B_i$ 's are usually discussed as independent parameters while the  $\tilde{m}_{L0i}^2$ 's and the tadpole conditions are often overlooked. Recall that imposing the correct tadpole equations is crucial in getting the correct physical scalars. If one is in favor of setting  $\tilde{m}_{L0i}^2$ 's to zero, a  $B_i$  value is then fixed by the corresponding  $\mu_i$ , and vice versa. However, in order to highlight some of the analytical features discussed and to enable an easy comparison with previous studies of other phenomenological implications of the  $B_i$  in the literature, we will first discuss the  $\mu_i$ 's and  $B_i$ 's separately as if they are independent. We will first single out a contribution involving a  $\mu_i$  by setting the  $B_i$  to zero and tuning  $\tilde{m}_{L0i}^2$  to satisfy the tadpole condition before solving for the spectra of the physical scalars. Likewise, we will tune a  $\mu_i$  to zero to single out a  $B_i$  effect. An interested reader can put the two otherwise related contributions, for example a  $\mu_3^* \lambda_{321}$  and a  $B_3^* \lambda_{321}$  contribution, together by imposing the tadpole equation and picking whatever  $\tilde{m}_{L0i}^2$  value deemed appropriate. We will also show a case of  $\tilde{m}_{L0i}^2 = 0$  for the  $\mu_1^* \mu_2$  contribution at the

end. Please be reminded that in the tadpole equation,  $B_i$  goes with a  $\tan\beta$  factor. For the same  $\mu_i$ ,  $B_i$  will then be suppressed by  $\tan\beta$ .

It is easy to see that under the strategy discussed, the additional RPV parameter combinations of interest are given by  $B_1^* \mu_2$ ,  $\mu_1^* B_2$ , and  $B_1^* B_2$ , together with  $B_k^* \lambda_{k21}$  and  $B_k \lambda_{k12}^*$ . These complete our list. Now, we go into each of these combinations of RPV parameters. Readers interested in more analytical details are urged to compare our discussions below with those presented in the previous section, the cross references to which are given inside square brackets ([ ]'s).

### A. The $\mu_k^* \lambda_{k21}$ or $\mu_k \lambda_{k12}^*$ contributions.

This is the most interesting case, because it involves both the bilinear and trilinear RPV couplings and also it is likely to give a much larger branching ratio. Later, we will see that the bounds obtained on such parameter combinations are comparable to what one could obtain by imposing a sub-eV bound on all neutrino mass contributions (see, for example, Refs [8,9,27]). Without loss of generality, we take the  $\mu_3^* \lambda_{321}$  combination for illustration. The dominant contribution comes from the last term of Eq.(19) as shown in Fig. 1 [also discussed in expression (20)]. This is confirmed by our exact numerical calculation. Another interesting contribution comes from the pure neutral gaugino with  $\mu_3^* \lambda_{321}$  coming in through the  $LR$ -slepton mixing. There are also the neutralino contributions without  $LR$ -slepton mixing, the exact analog of the chargino ones. In a generic region of the parameter space, the chargino-like loop result typically dominates over the neutralino-like loop result. We plot contours of the resulting branching ratio as a function of (real)  $\mu_3$  and  $\lambda_{321}$  in Fig. 5. The present experimental limit is also shown and the allowed region at 90% C.L. is shaded. The contours for the other three combinations of RPV parameters, each taken alone, are essentially the same. Recall that the corresponding dominating contribution for the two  $\mu_k \lambda_{k12}^*$  combinations comes in via the  $\mathcal{C}_{1nm}^R \mathcal{C}_{2nm}^{L*}$  part of  $A_2^R$  instead. The 90% C.L. upper limit on  $|\mu_k^* \lambda_{k21}|$  or  $|\mu_k \lambda_{k12}^*|$  (normalized by  $|\mu_0| = 100$  GeV) is given by

$$\frac{|\mu_3^* \lambda_{321}|}{|\mu_0|}, \quad \frac{|\mu_1^* \lambda_{121}|}{|\mu_0|}, \quad \frac{|\mu_3 \lambda_{312}^*|}{|\mu_0|}, \quad \frac{|\mu_2 \lambda_{212}^*|}{|\mu_0|} \quad < 1.5 \times 10^{-7}. \quad (29)$$

As to be explicitly illustrated below [and discussed with expression (21)], this kind of

contribution is insensitive to the  $\tan\beta$ . Recall that imposing a sub-eV bound for all neutrino mass terms obtainable from any RPV parameters (see, for example, Ref. [27]) gives  $\frac{|\mu_i|}{|\mu_0|} \cos\beta \lesssim 10^{-6}$ . A simple estimate of a 1-loop neutrino mass diagram from two  $\lambda$ -type couplings give the corresponding bounds  $|\lambda_{121} \lambda_{212}|, |\lambda_{321} \lambda_{312}| \lesssim 0.015$ , and  $|\lambda_{212}| \lesssim 0.008$ . These bounds are not very strong at all as factors of  $m_\mu$  and  $m_e$  are involved in the neutrino mass diagrams. Moreover,  $\lambda_{212}$  is the only parameter that is capable of giving rise to a 1-loop diagram just on its own, hence with a bound on itself alone. The other four  $\lambda$  couplings are otherwise bounded by 0.04 [28], from charged current processes and  $\tau$  decays. The  $\mu_i$  parameters typically have no strong bound apart from the one due to neutrino masses (see Ref. [14] for details), which is suggested but not mandated from the result of the super-Kamiokande experiment [29]. Hence, we can see that the bound we obtained here from  $\mu \rightarrow e\gamma$  is very important, especially in the large  $\tan\beta$  region where the neutrino mass bound is weakened. Further improvement in the  $\mu \rightarrow e\gamma$  experiment is capable of giving the best bound on the RPV parameters, or discovering the signal of th R-parity violation.

## B. The $\mu_1^* \mu_2$ contribution.

The contribution is dominated by the  $\mathcal{C}_{1nm}^R \mathcal{C}_{2nm}^{L*}$  term of  $A_2^R$  as depicted explicitly in Fig. 2 [*cf.* expression (22)]. The result obviously contains a “muon Yukawa” suppression. The same story goes for the contribution from the  $\mathcal{C}_{1nm}^L \mathcal{C}_{2nm}^{L*}$  part of  $A_2^L$ , depicted in Fig.4a [*cf.* expression (26)]. The latter is typically numerically smaller. We show contours of  $B(\mu \rightarrow e\gamma)$  in the real  $(\mu_1, \mu_2)$  plane in Fig. 6. The 90% C.L. upper bound on  $\mu_1^* \mu_2$ , normalized by  $|\mu_0|^2$  ( $|\mu_0| = 100$  GeV here), is

$$\frac{|\mu_1^* \mu_2|}{|\mu_0|^2} < 0.53 \times 10^{-4}. \quad (30)$$

Note that the bound weakens roughly by a factor of  $\frac{m_\mu}{\mu_0}$  compared with  $\frac{|\mu_3^* \lambda_{321}|}{|\mu_0|}$ , as expected. Though the bound looks weak compared with the sub-eV neutrino mass bound discussed above, it is still significant when compared with most of the other bounds on the  $\mu_1$  and  $\mu_2$  parameters, especially in the region of large  $\tan\beta$  [14].

### C. The contributions from two $\lambda$ -type couplings.

Here we have naively two classes of contributions, a class of  $\lambda^* \lambda$  diagrams and a class of  $\lambda \lambda$  or  $\lambda^* \lambda^*$  diagrams. The first class needs a chirality flip on the external muon line. We have a  $\lambda_{13k}^* \lambda_{32k}$  combination (for  $k = 1, 2, 3$ ) from the  $\mathcal{C}_{1nm}^R \mathcal{C}_{2nm}^{R*}$  part of  $A_2^R$  [*cf.* expression (27)], and a  $\lambda_{ij2}^* \lambda_{ji1}$  combination (for  $ij = 12, 13, 23$ ) from the  $\mathcal{C}_{1nm}^L \mathcal{C}_{2nm}^{L*}$  part of  $A_2^L$ . The first group must have a  $l_k^+$  running in the loop, while the second admits both a  $l_i^-$  and a  $l_j^-$  and hence gives a twice stronger result (with roughly degenerate  $L$  and  $R$  sleptons). The bounds obtained on appropriate combinations of  $\lambda \lambda^*$  are given in Table II, in which case we have deliberately used  $\tan\beta = 1$  (instead of 10, in order to keep the physical  $L$ - and  $R$ -handed slepton masses at about 100 GeV) to show the exact agreement with Ref. [19]. Note again the numerical bounds are roughly a factor of  $10^{-3}$  weaker than the  $\mu^* \lambda$ -type bound, as a result of the  $m_\mu$  factor.

On the other hand, a  $\lambda \lambda$  or  $\lambda^* \lambda^*$  diagram requires no chirality flip outside the loop. In the  $\lambda \lambda$  case, for example, we have to pick a  $\lambda_{h'2k'}$  to get the required reduction in  $L_\mu$  and a  $\lambda_{hk1}$  to get the increase in  $L_e$ . It is easy to see then that it is impossible to choose a combination of  $\lambda \lambda$  such that it does not cause further changes in any of the lepton-flavor numbers, unless more RPV parameters are involved. A term of the latter case has been discussed analytically [*cf.* expression (24)]. The same situation holds for  $\lambda^* \lambda^*$ . We will not further investigate such contributions here.

### D. The contributions involving the $B_i$ parameters

We have discussed above the implication of the tadpole equations relating the  $B_i$ 's to the  $\mu_i$ 's. Our numerical strategy isolates terms explicitly proportional to a  $B_i$  or a  $\mu_i$ . Here we discuss the contributions involving the  $B_i$ 's. First, there are combinations  $B_k^* \lambda_{k21}$  and  $B_k \lambda_{k12}^*$ . For  $B_k^* \lambda_{k21}$  an illustrative contribution has been discussed analytically in the previous section [*cf.* expressions (25) and (28)]. The bounds obtained on these combinations are shown in Table II. Contours of  $B(\mu \rightarrow e \gamma)$  in the real  $(B_3, \lambda_{321})$  plane are shown in Fig. 7. Understanding the result analytically is more complicated here. Our analysis does suggest more than one factor of Yukawa suppression, hence the weakness of the bound obtained.

Numerically, the part with external chirality flip from a  $\mathcal{C}_{1nm}^L \mathcal{C}_{2nm}^{L*}$  contribution [*cf.* expression (28)] can dominate over the part with the chirality flip inside the loop [*cf.* expression (25)] depending on  $\tan\beta$ . The overall bound looks stronger than the analytical estimate. This is to be explained by the larger loop function  $F_5$  with the much lighter muon propagator compared with that of a chargino, and the  $\tan\beta$  dependence. However, the relation between a  $B_k$  and a  $\mu_k$  and the weakness of the present result compared to the  $\mu_k^* \lambda_{k21}$  or  $\mu_k \lambda_{k12}^*$  result suggests that the  $B^* \lambda$ - or  $B \lambda^*$ - type contribution is really of less significance.

Next, we have the  $B_1^* \mu_2$  combination. Recall that according to our strategy, this is probed with  $\mu_1$  and  $B_2$  set to zero. It clearly has a “muon Yukawa” suppression [*cf.* expression (23)]. Numerically, the bound is similar to that on  $\mu_1^* \mu_2$ . The number shown in Table II actually looks better than the corresponding  $\mu_1^* \mu_2$  number. However,  $B_1$  comes in with a  $\tan\beta$  dependence. Therefore,  $\frac{|\mu_1|}{|\mu_0|}$  should be compared with  $\frac{|B_1 \tan\beta|}{|\mu_0|^2}$ , hence explaining the difference. Again, we give contours of  $B(\mu \rightarrow e \gamma)$  in the real  $(B_1, \mu_2)$  plane, in Fig. 8.

The analogous contribution of the type coming from  $\mu_1^* B_2$  has a “electron Yukawa” suppression. Numerically, it is confirmed to be much smaller. Likewise, we find no important contribution from an explicit  $B_1^* B_2$  combination. In fact, one obviously cannot make a simple  $\mu \rightarrow e \gamma$  diagram with a  $B_1^*$  and a  $B_2$  RPV insertions.

## E. Parameter Variations

In this section, we illustrate the effects of varying the input parameters on the bounds, using  $|\mu_3^* \lambda_{321}|$  and  $|\mu_1^* \mu_2|$  as examples. The results are summarized in Table III. Basically, the effects of varying the mass parameters  $(\mu_0, M_1, \tilde{m}_L^2, \tilde{m}_E^2)$  reflect on what particles are inside the loop of the dominant diagrams. In the case of  $|\mu_3^* \lambda_{321}|$ , the dominant diagram involves mainly the  $\tilde{l}_2^0$ , while the  $|\mu_1^* \mu_2|$  case involves the mixing between  $\tilde{l}_2^0$  and  $\tilde{l}_1^0$ . Therefore, varying  $\tilde{m}_E^2$  does not have much effect on the bounds while varying the corresponding entries in  $\tilde{m}_L^2$  changes the bounds significantly. Obviously, a large (relevant) scalar mass suppresses the  $\mu \rightarrow e \gamma$  amplitude and thus weakens the bounds [see parts (iii) and (iv)].

Increasing  $\mu_0$  and  $M_1 = \frac{1}{2} M_2$  essentially increases the chargino and neutralino masses [see parts (i) and (ii)]. Here, the variation of the bound is more complicated. For illustration, we show more details of the  $\mu_0$  variations in part (i). Taking  $|\mu_3^* \lambda_{321}|$  as an example, the bound

is most stringent for small  $|\mu_0|$ . However, for negative  $\mu_0$ , apart from the general weakening trend as  $|\mu_0|$  increases, there is an extra structure in the dominating chargino contribution, namely, there is a dip at  $\mu_0 = -M_2 \tan\beta$ , where it essentially vanishes. This is a special feature of the type of RPV contribution also observed in the similar contribution to neutron electric dipole moment [11]. For the relatively large value of  $\tan\beta$ , used here, however, this is already well inside the large  $|\mu_0|$  region where the pure gauge loop contribution becomes dominant. The latter case generally happens when the bino mass  $M_1$  is small relative to  $|\mu_0|$ . Note that the pure gauge loop contribution is independent of  $\mu_0$ . Apart from the dip mentioned, the dominant chargino contribution does decrease with increasing  $|\mu_0|$ , as shown in column 1 of Table III.

As for the  $|\mu_1^* \mu_2|$  case, the variation of the bound with  $|\mu_0|$  is more complicated. Unlike the previous case, the contribution has, analytically, an explicit chargino mass dependence [as shown by comparing expression (22) with expression (21)]. Hence, we do not expect a simple weakening of the result as  $|\mu_0|$  increases. Another important issue here is that there is more than one important piece of contribution of this type in most regions of the parameter space. For example, if we stick to setting  $B_1 = B_2 = 0$  as we do to obtain the numbers given in column 2 of Table III, we still have the pieces corresponding to Fig. 2 and Fig. 4a [*cf.* expressions (22) and (26)] in interference with one another. Besides, at very large  $|\mu_0|$  (and relatively small  $M_1$ ) the pure gauge-gauge term of the neutralino-like contribution is increasing and dominates over the chargino-like contribution.

In addition, we have shown in column 3 of the Table III, an interesting case with  $\tilde{m}_{I_{0i}}^2 = 0$  instead. Then the  $\mu_1^* \mu_2$ - and  $B_1^* \mu_2$ -type contributions exist simultaneously. As given in Eq.(10), we then have  $B_1 \tan\beta = \mu_0^* \mu_1$ , and the contribution of  $B_1^* \mu_2$  type such as that given by expression (23) comes along and interferes with that of the  $\mu_1^* \mu_2$ . Our result in Table II suggests that the  $B_1^* \mu_2$  type contribution is smaller than the  $\mu_1^* \mu_2$  type but are of the same order; a destructive interference of the two parts then weakens the overall result. Note that our analytical discussions in the previous section [*cf.* expressions (22) and (23)] indicate that the terms come in with a different sign. With larger  $|\mu_0|$ , the bounds shown in column 3 of the table are much weaker, because of a stronger cancellation as the  $B_1^* \mu_2$  term increases. This is mainly a result of the increase in the  $B_1$  value (for fixed  $\mu_1$ ), however,

the contribution from the term has more complicated dependence on the  $|\mu_0|$ . Similarly, the same increase in cancellation with larger  $\tilde{m}_L^2$ , as shown in the table can be understood from comparing the two terms. The results shown in column 3, hence, further illustrate the importance of the tadpole condition given by Eq.(10) emphasized throughout the paper.

Finally, we comment briefly on the  $\tan\beta$  dependence of the results, also illustrated in part (v) of Table III. From the table we can see that varying  $\tan\beta$  has only a little effect on  $|\mu_3^* \lambda_{321}|$  but a rather significant effect on  $|\mu_1^* \mu_2|$ . The lack of sensitivity to  $\tan\beta$  in the former case has been suggested in our analytical discussion [*cf.* expression (21)] and further confirmed over the range of the  $\tan\beta$  value. In the latter case, the numerical result shows that the bound is strengthened by a factor of  $\cos\beta$ . This simply illustrates the  $\frac{1}{\cos\beta}$  dependence of the Yukawa coupling  $y_{e_2}$ .

## V. CONCLUSION

In this paper, we have performed a comprehensive study on the radiative decay of muon ( $\mu \rightarrow e\gamma$ ) in the framework of the generic supersymmetric standard model (without R parity). We have identified a few combinations of a minimal number of RPV couplings contributing to the decay. Among them the most interesting are  $\mu_k^* \lambda_{k21}$  and  $\mu_k \lambda_{k12}^*$ . The upper bound on the combinations obtained from the experimental limit on  $\mu \rightarrow e\gamma$  is

$$\frac{|\mu_k^* \lambda_{k21}|}{|\mu_0|}, \frac{|\mu_k \lambda_{k12}^*|}{|\mu_0|} < 1.5 \times 10^{-7},$$

which is as stringent as the ones that can be obtained from the constraint of sub-eV neutrino masses. Note that different combinations of RPV parameters are involved in the generation of neutrino masses though. Furthermore, our result, in contrast to a similar result given in Ref. [20], has little sensitivity to  $\tan\beta$ .

Another combination,  $\mu_1^* \mu_2$ , contributing to  $\mu \rightarrow e\gamma$  involves the *LL*-slepton mixing. This contribution is identified for the first time. The upper bound on the combination obtained from the experimental limit on  $\mu \rightarrow e\gamma$  could be important, especially in the region of large  $\tan\beta$ . We have also discussed the related role of the soft SUSY breaking  $B_i$  parameters in the process.

Before closing we summarize the following important points :

(i) The combinations  $\mu_k^* \lambda_{k21}$  and  $\mu_k \lambda_{k12}^*$  participate directly in the *LR*-slepton mixings, while  $\mu_i^* \mu_j$  participate in the *LL*-slepton mixings. The combinations also highlight the major  $\mu \rightarrow e \gamma$  contributions. Under our formulation (SVP), the only RPV soft SUSY breaking parameters that contribute to (tree-level) slepton masses are the  $B_i$ 's and the  $\tilde{m}_{L0i}^2$ 's.

(ii) In relation to the RPV parameters (under SVP), the tadpole equations say that  $\{\mu_i, B_i, \tilde{m}_{L0i}^2\}$  for each  $i$  are not independent. This fact is often overlooked in the literature. In our study, we single out the contribution from  $\mu_i$  or  $B_i$  with a matching nonzero  $\tilde{m}_{L0i}^2$ . We have also illustrated a case with  $\tilde{m}_{L0i}^2 = 0$ , and thus combined the effects of both  $\mu_i$  and  $B_i$ . This case shows that there could be strong cancellations between them. Hence, the overall contribution from the bilinear RPV parameters only is tied up with how the tadpole equations among  $\{\mu_i, B_i, \tilde{m}_{L0i}^2\}$ 's are chosen to be satisfied.

## ACKNOWLEDGMENTS

This work was supported in part by the National Center for Theoretical Science under a grant from the National Science Council of Taiwan R.O.C., and in part by Academia Sinica.

## REFERENCES

- [1] See, for example, M. Gonzalez-Garcia, M. Maltoni, C. Pena-Garay, and J. Valle, Phys. Rev. **D63**, 033005 (2001).
- [2] See the recent review by Y. Kuno and Y. Okada, Rev. Mod. Phys. **73**, 151 (2001).
- [3] MECO collaboration, M.L. Brooks *et al.*, Phys. Rev. Lett. **53**, 1521 (1999).
- [4] MECO collaboration, L.M. Barkov *et al.*, Research Proposal E940 for an experiment at BNL (1997).
- [5] See, for a recent review, A. Masiero and L. Silvestrini, hep-ph/9711401.
- [6] G.F. Giudice and R. Rattazzi, Phys. Rep. **322**, 419 (1999).
- [7] J. Hisano, T. Moroi, K. Tobe, and M. Yamaguchi, Phys. Lett. **B391**, 341 (1997); J. Ellis, M.E. Gómez, G.K. Leontaris, S. Lola, and D.V. Nanopoulos, Eur. Phys. J. **C14**, 319 (2000); and references therein, for related scenarios within GUT frameworks.
- [8] K. Cheung and O.C.W. Kong, Phys. Rev. **D61**, 113012 (2000).
- [9] O.C.W. Kong, JHEP **0009**, 037 (2000).
- [10] Y.-Y. Keum and O.C.W. Kong, Phys. Rev. Lett. **86**, 393 (2001).
- [11] Y.-Y. Keum and O.C.W. Kong, Phys. Rev. **D63**, 113012 (2001).
- [12] See also, K. Choi, E.J. Chun, and K. Hwang, Phys. Rev. **D63**, 013002 (2001), which also discusses EDM as in Refs. [10,11]; however, among other differences, the RPV *LR*-scalar mixings are missing there.
- [13] K. Cheung, Y.-Y. Keum, and O.C.W. Kong, *IPAS-HEP-k011, manuscript in preparation.*
- [14] M. Bisset, O.C.W. Kong, C. Macesanu, and L.H. Orr, Phys. Lett. **B430**, 274 (1998); Phys. Rev. **D62**, 035001, (2000).
- [15] For more details in exactly the presently used notation see the upcoming review, O.C.W. Kong, *IPAS-HEP-k008, manuscript in preparation.*

[16] The complete expressions for all scalar masses are first given in Ref. [9]. However, the expression corresponding to Eq.(7) here was written with a typo — an extra numerical factor of 2.

[17] B. de Carlos and P.L. White, Phys. Rev. **D54**, 3427 (1996).

[18] D. Choudhury and P. Roy, Phys. Lett. **B378**, 153 (1996).

[19] M. Chaichian and K. Huitu, Phys. Lett. **B384**, 157 (1996).

[20] K. Choi, E.J. Chun, and K. Hwang, Phys. Lett. **B488**, 145 (2000).

[21] There are also related works on other aspects of LFV from R-parity violation. See, for  $\mu$ - $e$  conversion, K. Huitu, J. Maalampi, M. Raidal, and A. Santamaria, Phys. Lett. **B430**, 355 (1998); J.E. Kim, P. Ko, and D.-G. Lee, Phys. Rev. **D56**, 100 (1997); A. Faessler, T.S. Kosmas, S. Kovalenko, and J.D. Vergados, Nucl. Phys. **B587**, 25 (2000); A. de Gouv  a, S. Lola, and K. Tobe, Phys. Rev. **D63**, 035004 (2001), and Refs. [18,20] for some others.

[22] O.C.W. Kong, Nucl. Phys. B (Proc. Suppl.) **101**, 421 (2001).

[23] T. Banks, Y. Grossman, E. Nardi, and Y. Nir, Phys. Rev. **D52**, 5319 (1995).

[24] J. Hisano, T. Moroi, K. Tobe, and M. Yamaguchi, Phys. Rev. **D53**, 2442 (1996).

[25] Y. Grossman and H.E. Haber, Phys. Rev. **D59**, 093008 (1999); S. Davidson, M. Losada, and N. Ruis, Nucl. Phys. **B587**, 118 (2000); see also M. Hirsch, H.V. Klapdor-Kleingrothaus, St. Kolb, and S.G. Kovalenko, Phys. Rev. **D57**, 2020 (1998).

[26] Y. Grossman and H.E. Haber, hep-ph/9906310; S. Davidson and M. Losada, JHEP **0005** 021 (2000); see also Ref. [9].

[27] O.C.W. Kong, Mod. Phys. Lett. **A14**, 903 (1999); see also O.C.W. Kong, Phys. At. Nucl. **63**, 1083 (2000).

[28] See, for example, G. Bhattacharyya, Nucl. Phys. B (Proc. Suppl.) **52A**, 83 (1997); H. Dreiner, *Perspectives on Supersymmetry* (ed. G. Kane), p.462, (World Scientific 1999).

[29] Super-Kamiokande Collaboration, Y. Fukuda *et al.*, Phys. Rev. Lett. **81** 1562 (1998).

**Table captions :**

Table I — Basic input SUSY parameters for the numerical results presented. These values are adopted unless otherwise specified. Note that  $\tilde{m}_{L_{00}}^2$  corresponds to the soft mass square for  $H_d$ , in the MSSM language. Moreover, soft masses for  $H_u$  and  $B_0$  ( $\sim$  MSSM soft SUSY breaking  $B$  term) are not used as inputs, but are determined from  $\tilde{m}_{L_{00}}^2$  and  $\mu_0$  ( $\sim$  MSSM  $\mu$  term) through the tadpole equations for correct electroweak symmetry breaking.

Table II — Summary of bounds on various combinations of two R-parity violating parameters, normalized by  $|\mu_0| = 100$  GeV where appropriate, due to the experimental limit  $B(\mu \rightarrow e \gamma) < 1.2 \times 10^{-11}$  at 90% C.L. The input parameters are as in Table I, except for the limits on  $|\lambda\lambda^*|$  combinations in which case we have used  $\tan\beta = 1$  (as explained in the text).

Table III — Effects of parameter variations of interest, on the bounds of  $|\mu_3^* \lambda_{321}| \cdot (100 \text{ GeV})^{-1}$  and  $|\mu_1^* \mu_2| \cdot (100 \text{ GeV})^{-2}$ . Note that the fixed mass scale of 100 GeV is used for normalization to extract numerical bounds. The tadpole condition is chosen with  $B_i = 0$  in the second column of the bounds while  $\tilde{m}_{L_{0i}}^2 = 0$  is chosen in the last column.

**Figure captions :**

Fig. 1 — The R-parity violating chargino-like loop diagram.

Fig. 2 — Diagram with charged gaugino/higgsino mixing.

Fig. 3 — A diagram involving Majorana-like scalar mass insertion. 3a/ The diagram. 3b/ The seesaw origin of Majorana-like scalar masses for the “sneutrinos” explicitly illustrated.

Fig. 4 — Illustrative diagrams with chirality flip on the external muon line. 4a/. A charged gaugino loop. 4b/ A  $g - \lambda$  neutralino-like loop.

Fig. 5 — Contours of  $B(\mu \rightarrow e \gamma)$  in the (real) plane of  $(\mu_3, \lambda_{321})$ . The 90% C.L. allowed region is shaded.

Fig. 6 — Contours of  $B(\mu \rightarrow e \gamma)$  in the (real) plane of  $(\mu_1, \mu_2)$ . The 90% C.L. allowed region is shaded. Note that the approximation we used for the external lepton lines is less applicable at the right and top ends of the plot where the result should be read with caution.

Fig. 7 — Contours of  $B(\mu \rightarrow e \gamma)$  in the (real) plane of  $(B_3, \lambda_{321})$ . The 90% C.L. allowed region is shaded.

Fig. 8 — Contours of  $B(\mu \rightarrow e \gamma)$  in the (real) plane of  $(B_1, \mu_2)$ . The 90% C.L. allowed region is shaded.

## TABLES

TABLE I. Basic input SUSY parameters for the numerical results presented. These values are adopted unless otherwise specified. Note that  $\tilde{m}_{L00}^2$  corresponds to the soft mass square for  $H_d$ , in the MSSM language. Moreover, soft masses for  $H_u$  and  $B_0$  ( $\sim$  MSSM soft SUSY breaking  $B$  term) are not used as inputs, but are determined from  $\tilde{m}_{L00}^2$  and  $\mu_0$  ( $\sim$  MSSM  $\mu$  term) through the tadpole equations for correct electroweak symmetry breaking.

$M_1$ (GeV)	$M_2$ (GeV)	$\mu_0$ (GeV)	$\tan\beta$
100	200	100	10
$\tilde{m}_L^2$ ( $10^4$ GeV $^2$ )	$\tilde{m}_E^2$ ( $10^4$ GeV $^2$ )	$A_e$ (GeV)	
diag{2, 1, 1, 1}	diag{1, 1, 1}	100	

TABLE II. Summary of bounds on various combinations of two R-parity violating parameters, normalized by  $|\mu_0| = 100$  GeV where appropriate, due to the experimental limit  $B(\mu \rightarrow e \gamma) < 1.2 \times 10^{-11}$  at 90% C.L. The input parameters are as in Table I, except for the limits on  $|\lambda\lambda^*|$  combinations in which case we have used  $\tan\beta = 1$  (as explained in the text).

$ \frac{\mu_3^* \lambda_{321}}{ \mu_0 } $ , $ \frac{\mu_1^* \lambda_{121}}{ \mu_0 } $ , $ \frac{\mu_3 \lambda_{312}^*}{ \mu_0 } $ , or $ \frac{\mu_2 \lambda_{212}^*}{ \mu_0 } $	$< 1.5 \times 10^{-7}$
$ \frac{\mu_1^* \mu_2}{ \mu_0 ^2} $	$< 0.53 \times 10^{-4}$
$ \lambda_{321} \lambda_{131}^* $ , $ \lambda_{322} \lambda_{132}^* $ , or $ \lambda_{323} \lambda_{133}^* $	$< 2.2 \times 10^{-4}$
$ \lambda_{132}^* \lambda_{131} $ , $ \lambda_{122}^* \lambda_{121} $ , or $ \lambda_{232}^* \lambda_{231} $	$< 1.1 \times 10^{-4}$
$ \frac{B_3^* \lambda_{321}}{ \mu_0 ^2} $ , $ \frac{B_1^* \lambda_{121}}{ \mu_0 ^2} $ , $ \frac{B_3 \lambda_{312}^*}{ \mu_0 ^2} $ , or $ \frac{B_2 \lambda_{211}^*}{ \mu_0 ^2} $	$< 2.0 \times 10^{-3}$
$ \frac{B_1^* \mu_2}{ \mu_0 ^3} $	$< 1.1 \times 10^{-5}$

TABLE III. Effects of parameter variations of interest, on the bounds of  $|\mu_3^* \lambda_{321}| \cdot (100 \text{ GeV})^{-1}$  and  $|\mu_1^* \mu_2| \cdot (100 \text{ GeV})^{-2}$ . Note that the fixed mass scale of 100 GeV is used for normalization to extract numerical bounds. The tadpole condition is chosen with  $B_i = 0$  in the second column of the bounds while  $\tilde{m}_{L_{0i}}^2 = 0$  is chosen in the last column.

Parameter changes	Normalized numerical bounds		
	$\frac{ \mu_3^* \lambda_{321} }{(100 \text{ GeV})}$	$\frac{ \mu_1^* \mu_2 }{(100 \text{ GeV})^2}$	$\frac{ \mu_1^* \mu_2 }{(100 \text{ GeV})^2}$
	(with $B_i = 0$ )	(with $\tilde{m}_{L_{0i}}^2 = 0$ )	
Original inputs of Table I	$< 1.5 \times 10^{-7}$	$< 0.53 \times 10^{-4}$	$< 2.3 \times 10^{-4}$
(i) $\mu_0 = 500 \text{ GeV}$	$< 10 \times 10^{-7}$	$< 0.80 \times 10^{-4}$	$< 27 \times 10^{-4}$
$\mu_0 = 250 \text{ GeV}$	$< 5.8 \times 10^{-7}$	$< 1.1 \times 10^{-4}$	$< 14 \times 10^{-4}$
$\mu_0 = -100 \text{ GeV}$	$< 2.0 \times 10^{-7}$	$< 0.64 \times 10^{-4}$	$< 2.1 \times 10^{-4}$
$\mu_0 = -250 \text{ GeV}$	$< 6.8 \times 10^{-7}$	$< 1.1 \times 10^{-4}$	$< 8.8 \times 10^{-4}$
$\mu_0 = -500 \text{ GeV}$	$< 11 \times 10^{-7}$	$< 0.78 \times 10^{-4}$	$< 19 \times 10^{-4}$
(ii) $M_1 = \frac{1}{2}M_2 = 500 \text{ GeV}$	$< 9.3 \times 10^{-7}$	$< 3.7 \times 10^{-4}$	$< 16 \times 10^{-4}$
(iii) $\tilde{m}_L^2 = 20000 \times \text{diag}\{1, 1, 1, 1\} \text{ GeV}^2$	$< 2.2 \times 10^{-7}$	$< 1.3 \times 10^{-4}$	$< 18 \times 10^{-4}$
$\tilde{m}_L^2 = \text{diag}\{20000, 1000^2, 1000^2, 1000^2\} \text{ GeV}^2$	$< 2.4 \times 10^{-6}$	$< 840 \times 10^{-4}$	$< 44 \times 10^{-4}$
(iv) $\tilde{m}_E^2 = 20000 \times \text{diag}\{1, 1, 1\} \text{ GeV}^2$	$< 1.5 \times 10^{-7}$	$< 0.55 \times 10^{-4}$	$< 2.4 \times 10^{-4}$
$\tilde{m}_E^2 = \text{diag}\{1000^2, 1000^2, 1000^2\} \text{ GeV}^2$	$< 1.5 \times 10^{-7}$	$< 0.59 \times 10^{-4}$	$< 2.5 \times 10^{-4}$
(v) $\tilde{m}_L^2 = \text{diag}\{20000, 500^2, 500^2, 500^2\} \text{ GeV}^2$			
$\tilde{m}_E^2 = \text{diag}\{500^2, 500^2, 500^2\} \text{ GeV}^2$			
$\mu_0 = 100 \text{ GeV}, \tan \beta = 2$	$< 0.87 \times 10^{-6}$	$< 500 \times 10^{-4}$	$< 51 \times 10^{-4}$
$\tan \beta = 10$	$< 1.1 \times 10^{-6}$	$< 67 \times 10^{-4}$	$< 15 \times 10^{-4}$
$\tan \beta = 50$	$< 1.2 \times 10^{-6}$	$< 13 \times 10^{-4}$	$< 3.4 \times 10^{-4}$
$\mu_0 = 250 \text{ GeV}, \tan \beta = 2$	$< 2.2 \times 10^{-6}$	$< 450 \times 10^{-4}$	$< 150 \times 10^{-4}$
$\tan \beta = 10$	$< 3.1 \times 10^{-6}$	$< 88 \times 10^{-4}$	$< 50 \times 10^{-4}$
$\tan \beta = 50$	$< 3.4 \times 10^{-6}$	$< 18 \times 10^{-4}$	$< 12 \times 10^{-4}$
$\mu_0 = 500 \text{ GeV}, \tan \beta = 2$	$< 5.1 \times 10^{-6}$	$< 660 \times 10^{-4}$	$< 450 \times 10^{-4}$
$\tan \beta = 10$	$< 8.2 \times 10^{-6}$	$< 140 \times 10^{-4}$	$< 177 \times 10^{-4}$
$\tan \beta = 50$	$< 9.8 \times 10^{-6}$	$< 29 \times 10^{-4}$	$< 46 \times 10^{-4}$

## FIGURES

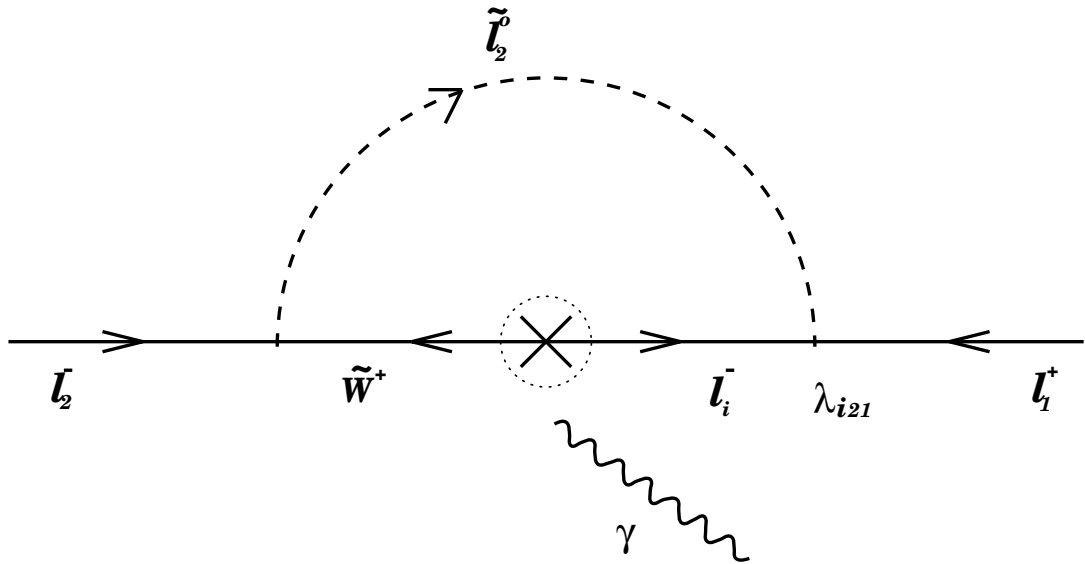


FIG. 1. The R-parity violating chargino-like loop diagram.

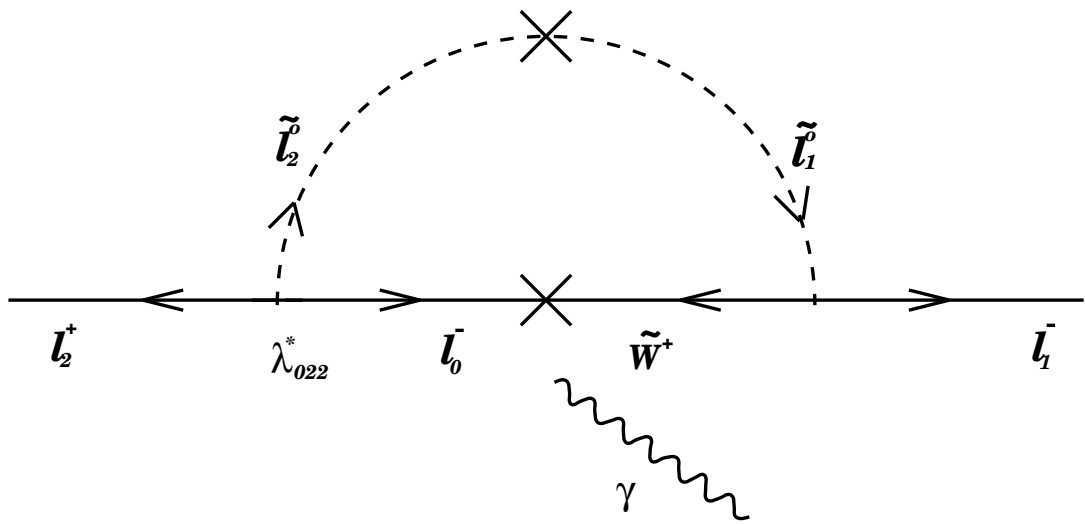


FIG. 2. Diagram with charged gaugino/higgsino mixing.

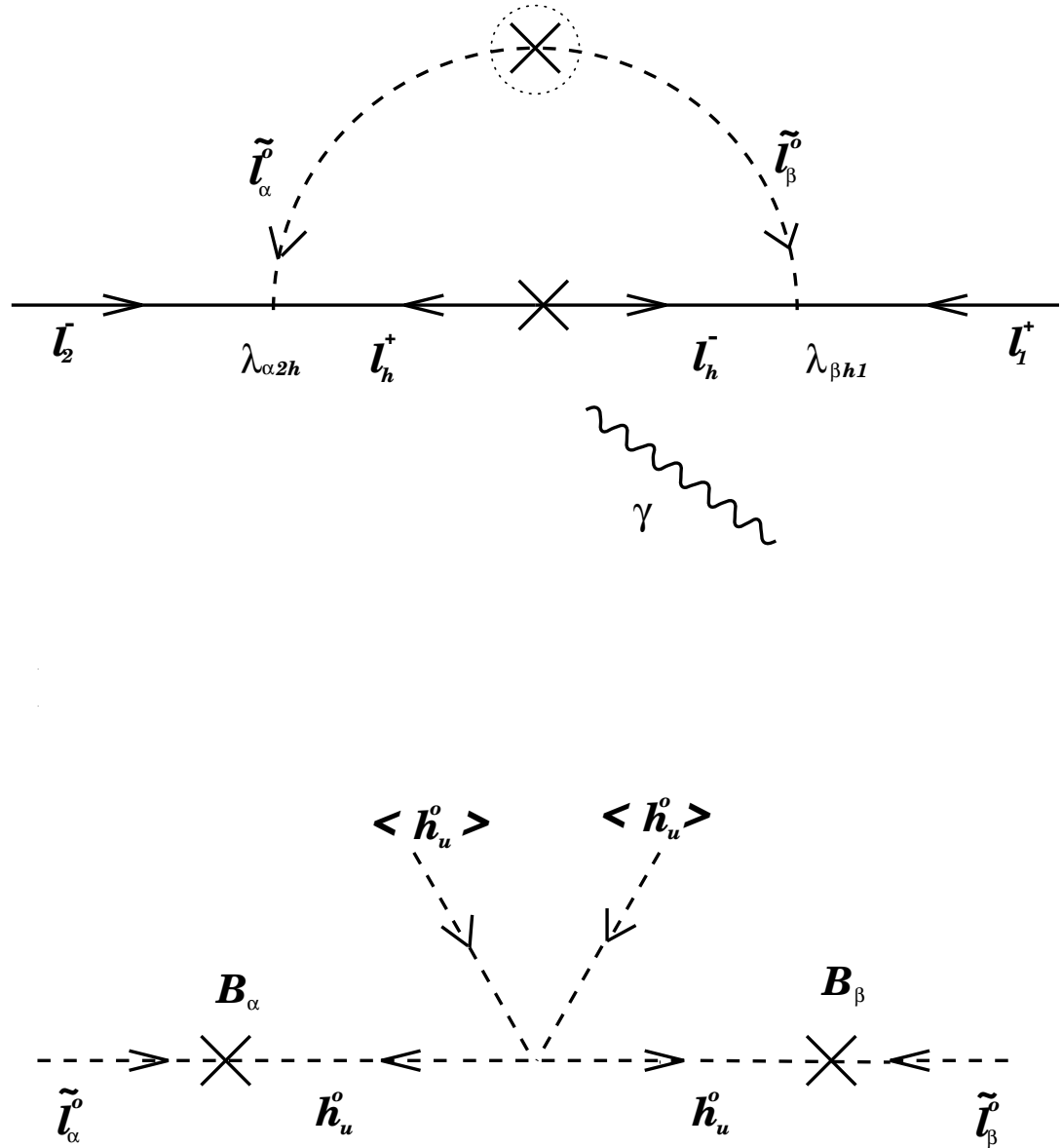


FIG. 3. A diagram involving Majorana-like scalar mass insertion. 3a/ The diagram. 3b/ The seesaw origin of Majorana-like scalar masses for the “sneutrinos” explicitly illustrated.

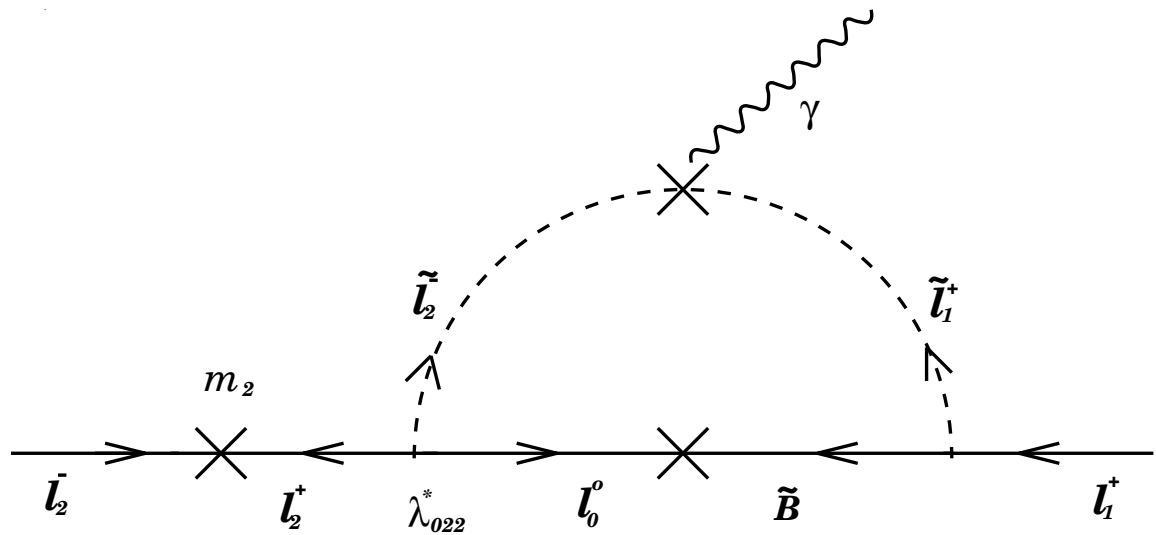
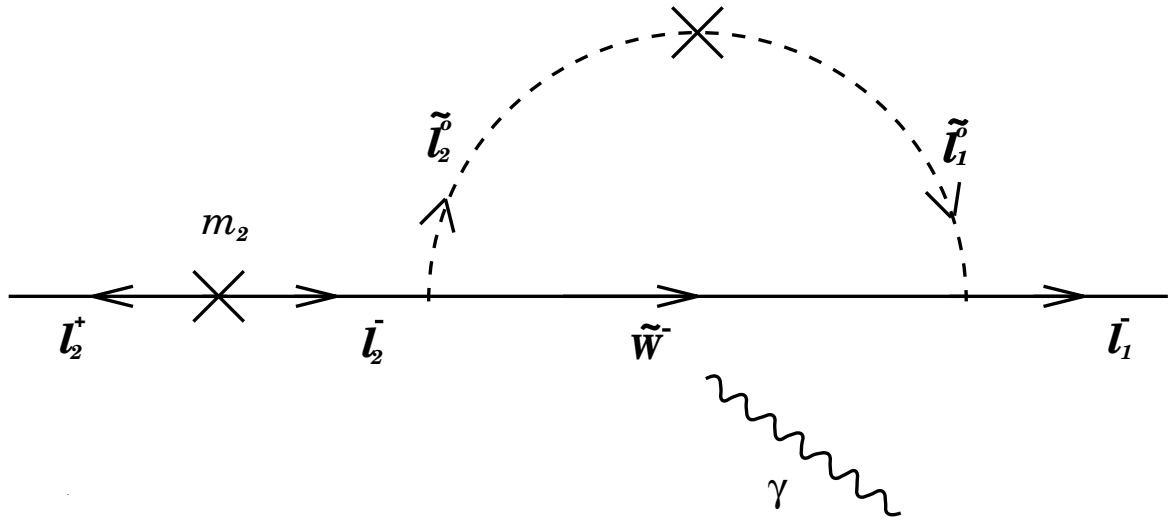


FIG. 4. Illustrative diagrams with chirality flip on the external muon line. 4a/. A charged gaugino loop. 4b/ A  $g \rightarrow \lambda$  neutralino-like loop.

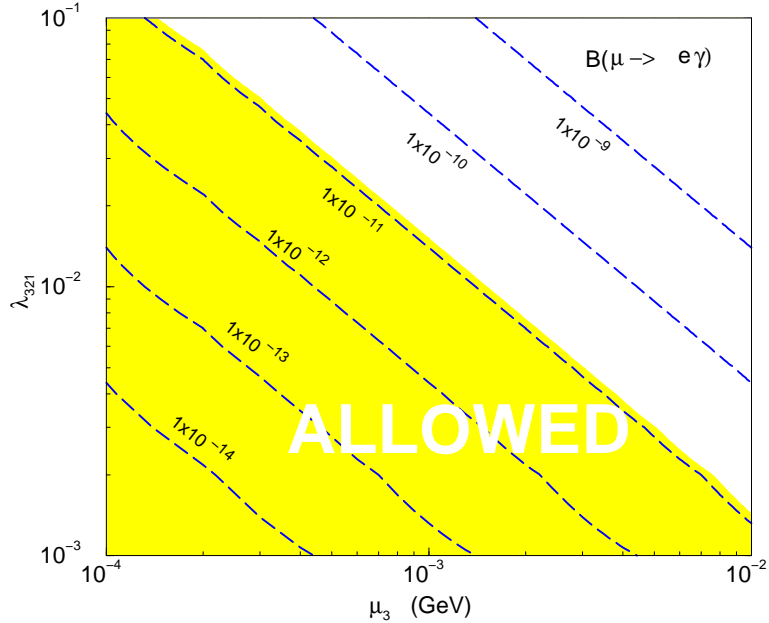


FIG. 5. Contours of  $B(\mu \rightarrow e \gamma)$  in the (real) plane of  $(\mu_3, \lambda_{321})$ . The 90% C.L. allowed region is shaded.

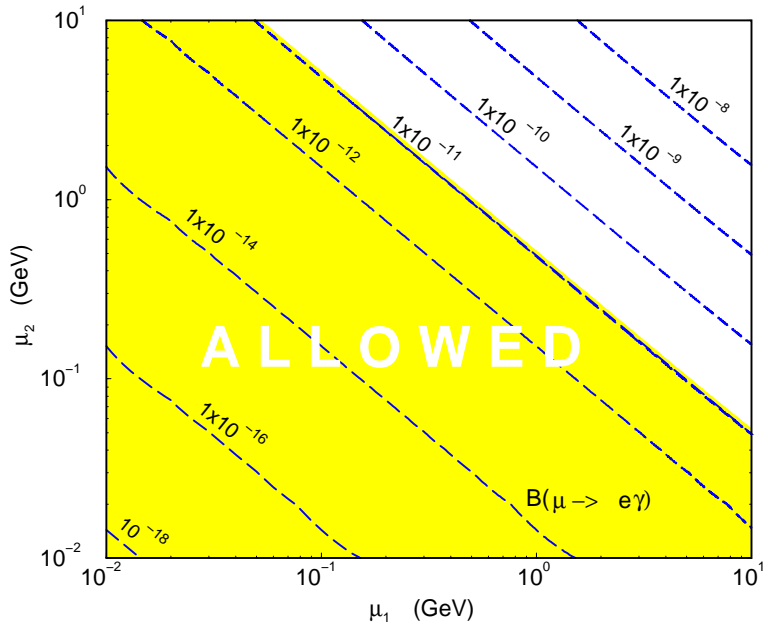


FIG. 6. Contours of  $B(\mu \rightarrow e \gamma)$  in the (real) plane of  $(\mu_1, \mu_2)$ . The 90% C.L. allowed region is shaded. Note that the approximation we used for the external lepton lines is less applicable at the right and top ends of the plot where the result should be read with caution.

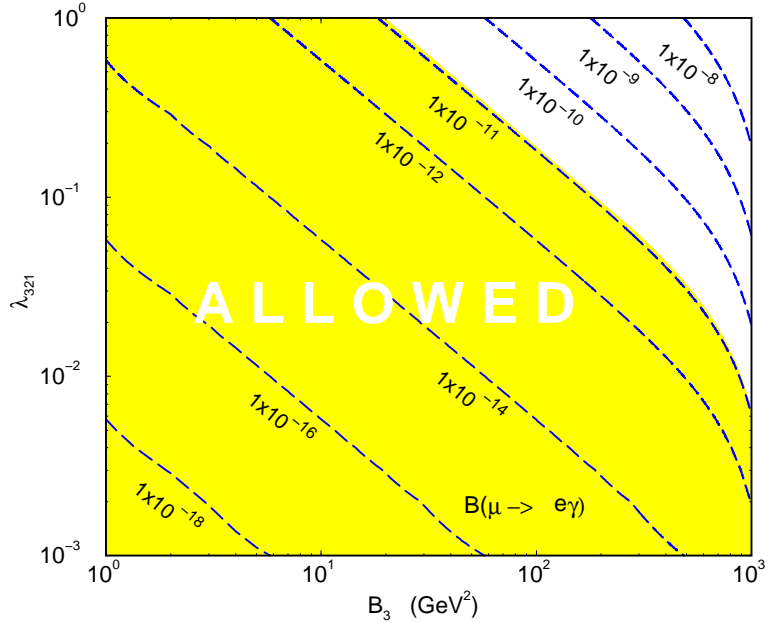


FIG. 7. Contours of  $B(\mu \rightarrow e \gamma)$  in the (real) plane of  $(B_3, \lambda_{321})$ . The 90% C.L. allowed region is shaded.

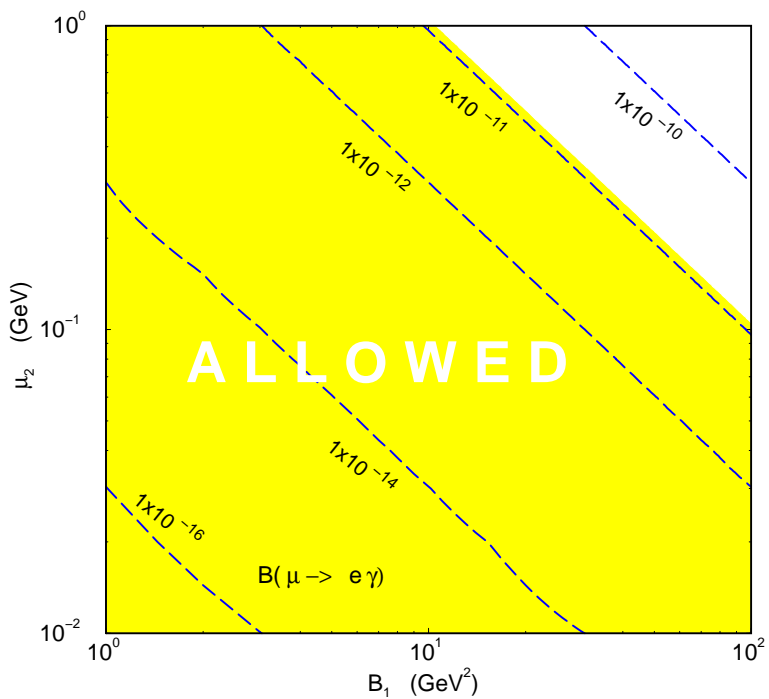


FIG. 8. Contours of  $B(\mu \rightarrow e \gamma)$  in the (real) plane of  $(B_1, \mu_2)$ . The 90% C.L. allowed region is shaded.